united nations
educational, scientific
and cultural
organization

international atomic
energy agency

the
abdus salam
international centre for theoretical physics

H4.SMR/1150 - 23

Fifth Workshop on Non-Linear Dynamics
and Earthquake Prediction

4 - 22 October 1999

Direct Simulations of the Stress Redistribtuion in the Scaling Organization of Fracture Tectonics (S.O.F.T.) Model

J.-L. Le Mouël

Institut de Physique du Globe de Paria,
Paris, France

submitted to *Geophys. J. Int.*

Direct Simulations of the Stress Redistribution in the Scaling Organization of Fracture Tectonics (S.O.F.T.) Model

C. Narteau[1], P. Shebalin[1,2], M. Holschneider[3], J.-L. Le Mouël[1] and C.J. Allègre[1,4]

[1] *Institut de Physique du Globe de Paris, 4, Place Jussieu, Paris, Cedex 05, 75252, France*

[2] *International Institute of Earthquake Prediction Theory and Mathematical Geophysics, Warshavskoye shosse, 79, korp 2, Moscow 113556, Russia*

[3] *Centre de Physique Théorique, CNRS, Case 907, F-13288 Marseille, France*

[4] *Université Paris VII, 4, Place Jussieu, 75252 Paris Cedex 05, France*

SUMMARY

A time dependent stochastic process with three states (solid, broken and moving) is considered in a hierarchical system made of embedded cells of increasing levels. An earthquake of a given scale k is associated with the moving state of a cell of level k and results from the coherent self-organization of fractures of lower scales. A direct cascade of stress redistribution generates small scale stress heterogeneities in the neighborood of the active fracture. An interesting feature of the model is that the size of the domain where stress redistribution takes place grows proportional to the length of the fracture. In the framework of the general model, inspired by the progress in the use of the renormalisation techniques in approaching critical point phenomena, we independently study a "fracturation" submodel and a "friction" one. These submodels are two states models which act on different time scales. In the "friction" submodel which comprises broken and moving states, the transitions between these two states are associated with a stick-slip behaviour in a completly fractured fault zone. In the "fracturation" submodel which comprises solid and broken states, we model the brittle behaviour of rock material. In both models we

3W?●8ΔJÇ#◌=◎obtain a spatio-temporal clustering of earthquakes, realistic aftershocks sequences whose
Σ C. Narteau et al.

obtain a spatio-temporal clustering of earthquakes, realistic aftershocks sequences whose frequencies decrease respects the modified Omori law, and a frequency-magnitude relationship which respects the Gutenberg-Richter law. We show that the model behaviour is controlled by the stress heterogeneity in the fault zone, evidence a relationship between the periodicity of the largest earthquakes and the b-value, and indicate how the different physical ingredients underlying each submodel can be gathered in a more general model.

Key words: seismicity – hierarchical system – cascade – fracturation & friction – Omori law – heterogeneity.

1 INTRODUCTION

Earthquakes mainly occur in fault zones, boundaries between tectonic plates, and result from the relative large scale motions of these plates. These fault zones include a large number of faults which interact together (Harris 1998) to accomodate the large scale deformation. Most faults are schematically characterized by two phases during their history: an aseismic long time period, without relative motion of the two sides of the fault, separated by short periods of seismic activity (foreshocks-main shock-aftershocks sequence, swarm of small earthquakes). Other faults produce aseismic slip (slow earthquakes, creep) with a large number of microearthquakes. Collected information has revealed a spatio-temporal clustering of the seismicity and different statistical behaviours. Such are the Gutenberg-Richter power law of the size-frequency statistics (Gutenberg & Richter (1944) who recall that "*earthquakes may be expected to occur in the future, as in the past*"), the Omori law which describes the aftershocks frequency decrease (Omori 1894; Utsu, Ogata & Matsu'ura 1995) as well as the foreshocks frequency increase (Papazachos 1975), the relation between the energy radiated by an earthquake and its size (Kanamori & Anderson 1975).

Fracturation process determines the length of the major fault as well as the distribution of cracks at all scales. Friction can then play its part in the fractured zone. In a recent past, the developpment of a constitutive law of rock friction (Dieterich 1979) gives a frictionnal interpretation of a large range of deformation phenomena (Scholz 1998) associated with pre-existing fractures: creep (Scholz 1990), seismic regimes (Marrone & Scholz 1988; Tse & Rice 1986), aftershocks (Dieterich 1994), nucleation phase (Campillo & Ionescu 1997), seismic cycle (Ben-Zion 1996; Rice & Ben-Zion 1996), coseismic phase (Cochard & Madariaga 1994). Nevertheless, shear fractures do not always occur along pre-existing structures and the rupture could be initiated in or propagate into intact or healed bulk rock. For long time periods, and to include the large scale heterogeneity of rheological

rock properties, the analysis of the rupture of a fault zone has to include the fracture mechanism (Yamashita & Ohnaka 1991).

Earthquakes genesis can also be tackled with tools of non linear physics (e.g. Dubois & Gvishiani (1998)). The seismogenic layer of the Earth has been considered to exhibit a state of "self organized criticality" (S.O.C.) (Bak & Tang 1989; Main 1997). A large number of phenomenological models (see references in Main (1996)) reproduce this statistically stationary state characterized by spatial and temporal correlation functions with a power law behaviour. This is also obtained by Correig, Urquizú & Vila (1997) who use a cellular automatom to model the aftershocks frequency decrease. Discarding the state of S.O.C., Knopoff (1997) suggests that the healing of cracks and the rate of healing have to be taken into account in a fault zone (Marrone 1998) to obtain an understanding of the self-organization of earthquakes. The Burridge-Knopoff (B.K.) model (Burridge & Knopoff 1967) models a fault by a spring-block system lying between two rigid tectonic plates; it reproduces the Gutenberg-Richter law. Including a relaxation time, Hainzl, Zöller & Kurths (1999) also reproduce the Omori law and the increase with time of the foreshocks frequency.

Our approach can be compared with renormalisation techniques used for other examples of critical point phenomena in different areas of physics (Binney et al. 1992). It can be seen as a link between the physical approachs recalled above, the B.K. multiblocks approach, and the scaling approaches to earthquakes. In our previous work (Allègre et al. 1995, 1998) a fault zone is modeled by a hierarchical system made of embedded cells. Earthquakes which occur within the fault zone are the result of tectonic loading. Each earthquake is a critical phenomenon which is the expression of a self-organization of fractures at all scales. This view is supported by field observation (King 1983) or laboratory experiments (Tapponnier & Brace 1976). The potential elastic energy coming from outside increases the density d of cracks at the lowest level; the density of cracks at higher levels is directly calculated from d by a criterion of coherent organization of fracture (we call it the S.O.F.T. rule; Allègre, Le Mouël & Provost (1982)). The corner stone of this former approach (that we will call integral approach) is the appearance of a critical density of cracks d_c: the density of cracks versus d at a given level k tends toward a (Heaviside) step-function $H(d - d_c)$ with increasing k. The whole organization process, through all the scales, is completed during a chosen unit of time and, after an event, part of the energy is redistributed in the non broken part of the medium while another part is emitted by acoustic waves or consumed by friction. With this kind of approach it is possible to obtain some characteristic classes of seismic behaviours (seismic noise, swarms, earthquakes with or without precursors; Allègre et al. (1995)), a typical time distribution of aftershocks (Allègre et al. 1998), and also, following somewhat different lines, to generate an algorithm of prediction based on the variation of the local slope of the

magnitude-frequency relationship (Blanter, Shnirman & Le Mouël 1997). A large range of critical behaviours is also observed depending on the fracture criterion (Shnirman & Blanter 1999).

The present model is an implementation and an improvement of the integral approach; we now study a hierarchical system of identified cells, each of them being in one of a given number of states. Non stationary transition rates between the various states and a stochastic process at the lowest scale define the location in time and space of each transition. We can determine the origin (in time and space) of the modeled structures (fractures) and their history on different time scales. Our basic assumptions are as follows: the rupture can be initiated by the fracturation of a solid part of the medium (asperity) or take place in a broken part through the friction process. The rupture can propagate until it is stopped by more solid parts (barriers; Aki (1984)). These more solid parts of the medium favor in turn the loading up of the shear stress which can be eliminated by both earthquakes or creep processes. We also include healing of cracks and a direct cascade (from higher levels to lower ones) of stress redistribution after each event. The stress redistribution generates small scale stress heterogeneities from which one can compute the stress field at different scales. A time delay is precisely defined using the shear wave velocity, and this implies a more sophisticated S.O.F.T. rule with memory. We can describe in terms of a cascade model (Ellsworth & Beroza 1995) the nucleation phase and the coseismic phase of an earthquake. A low frequency of the stick-slip behaviour at the lowest scale can be associated with the seismicity along creeping faults or during slow earthquakes. We eventually generate long duration synthetic catalogs containing time, magnitude and location of the events.

We will rather systematically compare the model results with seismicity observations. We are aware that confrontation of theory and experience cannot, in the present case, lead to what could be called a proof of the validity of our approach. We will come back to this point in sec. 5.

2 THE GENERAL MODEL

In this paper we use the integral approach of the S.O.F.T. model (Allègre et al. 1995, 1998) as a starting point for a stochastic time dependent model of a fault zone in which we incorporate the stress redistribution following seismic events. In a homogeneous system, indeed, the redistribution of stress at different scales and locations is the main cause of the heterogeneous distribution of cracks.

We propose first a general model which supposes the co-existence of "*friction*" along existing fractures, and "*brittle fracture*" of the solid parts of the medium ("asperities", "barriers"). These two rupture mechanisms are then independently studied, their characteristic behaviours described, as well as the seismic phenomena they are associated with. The first variant, the "*friction*" model, starts from a completly fractured state (all the cells, at all scales, are broken) and there is no healing process. In the second variant, the "*brittle fracture*" model, we neglect friction and assume that only the solid

(unfractured) part of the medium concentrates the elastic potential energy; rupture is initiated in a solid part and can propagate in the fractured part. The rupture threshold is constant for each model but larger in the case of the fracturation process.

[Figure 1 about here.]

Let us present our basic assumptions. The seismicity generation process takes place in a certain domain of a fault zone. This domain is modeled by an abstract hierarchical system composed of embedded $\mathcal{D}$-dimensional cells in the way explained in Fig. 1 (with $\mathcal{D} = 2$): the highest level is associated with one cell and is subdivided in $\mathcal{R}^{\mathcal{D}}$ cells of the same shape, $\mathcal{R}$ being the renormalization factor. For each of these cells we repeat the same operation until we obtain a hierarchical sytem of cells with $\mathcal{K}$ different scales. Let $k = 0$ be the smallest scale, and $k = \mathcal{K}$ the largest. Our model is based on the simultaneous consideration of all scales. It is important to stress that our hierarchical system of cells does not represent a system of solid or quasi-solid blocks. Each cell at each level rather represents a boundary between two blocks, or a fracture. It can then be associated with a possible fault plane which is localized somewhere within this cell. Each cell (crack) will interact with neighboring cells (cracks) and possibly create a fracture at larger scale in a larger cell.

We suppose that, as the result of the long term, large scale, tectonic fracturing process, our system is polarized in the direction of the fault plane of the largest possible fracture. We shall call this direction the "*main direction*". For the sake of simplicity, we suppose that the rupture propagates only along this "*main direction*". We only study the case of simple shear stress loading, which corresponds to a strike-slip earthquake faulting mode. This idealized geometry can be modeled by a 2-dimensional hierarchical system which represents a plane (Fig. 1, $\mathcal{D} = 2$). The source of this loading is the motion of two tectonic plates in opposite directions. We suppose a constant rate of motion and a constant normal stress; accordingly, shear stress would increase constantly but for the strain energy dissipated by earthquakes or non-elastic deformations (creep, plastic deformation). The process is associated on the one hand with a discontinuous energy dissipation, and, on the other hand, with a temporal variation of the average shear stress. Furthermore, the complex geometry of fracturing creates a heterogeneous stress distribution. We neglect the heterogeneity of elastic and fragile properties of the medium.

According to Bâth (1974), the duration of an earthquake, τ, defined as the rupture time, has the following empirical dependence versus magnitude:

$$\log \tau = \log(\frac{\mathcal{L}}{v_r}) = 0.5M + 1.9 \tag{1}$$

where $\mathcal{L}$ is the earthquake fault length, v_r the fracturation velocity, and M the earthquake magnitude. A larger earthquake has a longer duration; while a part of the earthquake fault continues to move, some others have already stopped, and during the fracturation process it is impossible to determine

the final magnitude of the event. In this paper we consider a constant rupture velocity of the order of magnitude of the shear wave velocity.

We now expose in more precise terms the stochastic dynamical system that we study in this paper.

2.1 The hierarchical system

The hierarchical system is obtained, as said above, by dividing a $\mathcal{D}$-dimensional cell into $\mathcal{R}^{\mathcal{D}}$ smaller cells and so on, $\mathcal{K}$ times. There are thus $n(k) = \mathcal{R}^{\mathcal{D}(\mathcal{K}-k)}$ cells at scale k, $k = 0, \ldots, \mathcal{K}$. Let us denote by $C = C_i^k$, $i \in \{1, 2, ..., \mathcal{R}^{\mathcal{K}-k}\}^{\mathcal{D}}$ the $\mathcal{R}^{\mathcal{D}(\mathcal{K}-k)}$ cells of scale k and by $\Lambda_j(C_i^k)$, $j < k$, all the cells of scale j contained in C_i^k (Fig. 1). In case $j \geq k$, $\Lambda_j(C_i^k)$ stands for the unique cell of scale j in which C_i^k is included. Thus $\Lambda_k(\Lambda_{k+1}(C))$ are all the cells of level k contained in the same cell of the next larger scale cell that contains C. At each moment any cell can be in three possible states :

(i) solid (non fractured or non broken) : state **s**.

(ii) broken (locked by friction, fractured and motionless) : state **b**.

(iii) moving (active) : state **m**.

$$C \in \{s, b, m\}.$$

The characteric length of a cell of scale k is

$$l(k) = l_0 \mathcal{R}^k. \tag{2}$$

where l_0 is the length of the cells of the elementary level. For a given cell of scale k, to be in the state solid means that there is no fracture of length $l(k)$ in it. On the contrary, a broken or a moving cell have fractures of size $l(k)$. A broken cell is weaker than a solid one, and consequently a smaller shear stress suffices to initiate its motion. A moving cell corresponds to a rupture of size $l(k)$ taking place. The propagation of this rupture is not instantaneous but rather takes a characteristic time, ΔT^k. Due to our assumption of a constant rupture velocity this means

$$\Delta T^k = \frac{l(k)}{v_r} \tag{3}$$

(see however section 3.2). After defining the state transitions, we describe the smallest scale dynamics, then the inverse cascade (from small scales to large scales) of rupture (fracture and friction), and finally the dynamics of the direct cascade (from large scales to the smallest scale) of stress redistribution.

[Figure 2 about here.]

2.2 The state transitions

There are 4 possible transitions for the cells (c.f Fig. 2):

$$s \rightarrow m \tag{4}$$

$$b \rightarrow m \tag{5}$$

$$m \rightarrow b \tag{6}$$

$$b \rightarrow s \tag{7}$$

"fracturation": the $s \rightarrow m$ transition is associated with a fracturation process. We model by this transition the brittle behaviour of rocks under a given state of stress: appearance of new cracks, crack development and cracking along old healed cracks. We do not detail any precise failure mechanism but just consider the initiation of cracks and their propagation along distance $l(k)$. This phenomenon implies a motion of both sides of the crack.

$b \rightarrow m$ and $m \rightarrow b$ are the two transitions that constitute the stick-slip process.

"friction": the $b \rightarrow m$ transition is associated with a friction process. The slip takes place on an irregular fractured surface (micro-fault plane). During all the broken state time, the opening of the crack is kept constant; we neglect the complex geometry of this pre-existing crack.

"stopping": corresponding to a stress drop, the $m \rightarrow b$ transition represents the stopping of both rupture processes (friction and brittle). The locally accumulated shear stress is released by the motion of the sides of the old or of the new crack. When the release reaches a large enough amount, the motion stops and the sliding surface becomes a static microcrack (broken state).

"healing": The $b \rightarrow s$ transition is associated with a healing process. This phenomenon results from physico-chemical processes at the microscopic scale in rocks: compaction in presence of fluid, grain growth and crack cristallization. We consider that a healed crack has the same mechanical properties as a never fractured part of the rock material.

The two other transitions do not occur since a solid cell first starts moving and stays sliding during ΔT^0 before it becomes broken (recall that broken means fractured but not moving); moreover a moving cell can obviously not become solid without stopping.

2.3 The smallest scale

We define the whole process in terms of non stationary transition rates between the various states. In general, these transition rates will depend on the present state of a cell and on its past, as well as on the past of its neighbor cells. At the smallest scale it depends in addition on the local stress, which in turn changes due to seismic events and global large scale loading. We come to the details.

We attach to each cell $C = C^0$ a real number, $\sigma = \sigma(C, t)$, which varies with time and represents

the local accumulated stress. The dynamics at the smallest scale is given by a time dependent stochastic process. In the following we write $\alpha_{u\to v}$ for the variable transition rate from state $u \in \{s, m, b\}$ to $v \in \{s, m, b\}$. Recall what this means: given that a cell is in state u, the probability that it undergoes a transition towards the state v in the infinitesimal time interval dt is $\alpha_{u\to v}dt$. The transition rate for $b \to s$ is fixed to some constant value β independent of the state of the system:

$$\alpha_{b\to s} = \beta, \tag{8}$$

we neglect the complex dependency on physical parameters as temperature, local pressure, amount of fluid, of the geochemical healing process ($b \to s$).

The transition rate $s \to m$ depends on the local stress only. For its dependency on the local shear stress we use the following expression ($\sigma = \sigma(C, t)$)

$$\alpha_{s\to m}(\sigma) = \begin{cases} 0 & \text{for } \sigma \leq \sigma_s \\ k_s(\dfrac{\sigma - \sigma_s}{\sigma_s})^{\delta_s} & \text{for } \sigma > \sigma_s \end{cases} \tag{9}$$

where σ_s is the fracture threshold, k_s is a constant with the dimension of the inverse of a time and δ_s is some phenomenological material constant.

The transition rate $m \to b$ is deterministic:

$$\alpha_{m\to b}(t) = \delta(t - [t_0 + \Delta T^0]). \tag{10}$$

Here $t_0 = t_0(t)$ is the time when the cell became moving for the last time and ΔT^0 is a time delay (see eq. 3). Thus in other words, a cell that has started to move becomes broken (and not moving) allmost surely after a time ΔT^0. A constant rate of stress release (stress drop) during ΔT^0 justifies this assumption.

The transition rate $b \to m$ has two contributions corresponding to two different possible mechanisms.

$$\alpha_{b\to m} = \alpha^1_{b\to m} + \alpha^2_{b\to m} \tag{11}$$

The first is the analogue of the transition $s \to m$. It is a spontaneous random transition that depends only on the actual local stress in the cell.

$$\alpha^1_{b\to m}(\sigma) = \begin{cases} 0 & \text{for } \sigma \leq \sigma_b \\ k_b(\dfrac{\sigma - \sigma_b}{\sigma_b})^{\delta_b} & \text{for } \sigma > \sigma_b \end{cases} \tag{12}$$

where now σ_b the friction threshold, k_b is a constant with the dimension of the inverse of a time and δ_b is some phenomenological material constant.

The second contribution corresponds to a transition that is induced by some neighbor cell (intra-scale propagation): a broken cell starts moving a time ΔT^0 (intra-scale growth of "fracturation") after a neighbor solid cell along the main direction started moving (nucleation of the "fracturation"). In more

precise terms, a **broken** cell becomes **moving** at time t if, at time $t - \Delta T^0$, one of its "neighbours" underwent a transition **solid-moving**. Here the "neighbour" cells of C are those in the set $\Lambda_0(\Lambda_1(C))$ (the $\mathcal{R}^{\mathcal{D}}$ cells within the same cell of scale 1 that contains C) which lie along the main direction with respect to C. Thus

$$\alpha^2_{b\to m}(t) = \delta(t - [t_0 + \Delta T^0]), \tag{13}$$

where now $t_0 = t_0(t)$ is the latest time point when a neighbor cell (in the above sense) underwent a transition $s \to m$. Such an *intra-scale propagation* will also hold for scales $k > 0$ (see below). The intra-scale propagation direction is the same as the direction intervening in the critical rule of the inter-scale rupture propagation (S.O.F.T. rule) which we detail in the next section.

In our numerical experiment we will denote $\pi(t)$ the sum of all the transition rates, at time t, at the elementary level of the hierarchical system. It is a measure of the actual stochastic activity in our system.

2.4 The inverse cascade of "fracturation","friction" and "blocking"

In previous papers on the S.O.F.T. model (Allègre et al. 1995, 1998), only solid and broken cells were considered in the hierarchical system. The transfer of fracturation from lower levels to upper ones (inverse cascade) was determined by a simple rule: if at least one straight line (following the main direction) of cells ($\mathcal{R}$ cells) of level k is composed only of broken cells, the corresponding cell of level $k+1$ is also broken (Fig. 3). In this case the state of all cells at all levels is entirely determined by the configuration at the smallest scale. At each time, the state of larger scales is a function of the instantaneous picture at the smallest scale. The different scales do not have any proper dynamics since they are, so to speak, "slaves" of the smallest scale.

[Figure 3 about here.]

Here we consider a system with a memory, a next neighbour correlation (c.f. above the intra-scale propagation) and a more elaborated S.O.F.T. rule. The new S.O.F.T. rule associates with a cell C at level k a "virtual" state which is a function of the configuration of the $\mathcal{R}^{\mathcal{D}}$ cells in $\Lambda_{k-1}(C)$. However, the "real" state of C will also depend on its history and on its next neighbours. No additional stochasticity is introduced at scales larger than the elementary scale ($k = 0$).

The new S.O.F.T. rule is as follows: $C = C^k_i$ is "virtually" **moving** if the **moving** cells in $\Lambda_{k-1}(C)$ are in a critical state with respect to the classical S.O.F.T. rule. C is "virtually" **broken** if the **broken** cells in $\Lambda_{k-1}(C)$ are in a critical state with respect to the classical S.O.F.T. rule. In case of a conflict between both rules the **moving** rule prevails. In all other cases C is "virtually" **solid**.

The rules for the various transitions of a cell of level k are as follows.

(i) Suppose C is in the state **solid**. It undergoes the transition **solid** $\rightarrow$ **moving** if it becomes "virtually" **moving**.

(ii) Suppose C is in the state **moving**. It undergoes the transition **moving** $\rightarrow$ **broken** at time t if it started to move at time $t - \Delta T^k$. That means that, once it starts moving, it stays moving for ΔT^k (according to eq. 1) before it becomes **broken**. Therefore it may happen that, while a cell is **moving**, the smaller scale configuration changes in such a way that it becomes "virtually" non **moving**; nethertheless the cell keeps moving till the time ΔT^k is completed. This is the main difference between our new concept with memory and the classical static S.O.F.T. rule: if, as in Allègre et al. (1995), the **moving** state at all scales $k \neq 0$ is a function of the instantaneous configuration at scale $k = 0$, the lifetime of the **moving** cells (the average duration of the **moving** state during the numerical experiment) can be smaller for higher degrees. Let us detail this difference with the most simple example: $\mathcal{R} = 2, \mathcal{K} = 1, \mathcal{D} = 1$. The hierarchical system is made of two cells C_1^0 and C_2^0 of level 0, aligned along the main direction and included in the unique cell C_1^1 of level 1. If the cell C_1^0 starts to move at t_1 for an interval of time ΔT^0, and the cell C_2^0 starts to move at $t_2 \in [t_1; t_1 + \Delta T^0]$ for an interval of time ΔT^0, C_1^1 is **moving**: (a) during $[t_2; t_1 + \Delta T^0]$ in the case of the static S.O.F.T. rule; (b) during $[t_1; t_1 + \Delta T^1]$ in the present case of the S.O.F.T. rule with memory.

(iii) Suppose C is in the state **broken**. It undergoes the transition **broken** $\rightarrow$ **solid** if it becomes "virtually" **solid** (hierarchical geometric blocking). Let us extract from the most simple example (as above $\mathcal{R} = 2, \mathcal{K} = 1, \mathcal{D} = 1$) an interesting behavior: if C_1^0 is **broken** during $[t_1; t_1 + \Delta t_1^\beta]$ and C_2^0 is **broken** during $[t_2; t_2 + \Delta t_2^\beta]$ with $t_2 \in [t_1; t_1 + \Delta t_1^\beta]$, C_1^1 is only **broken** during $[t_2; min(t_1 + \Delta t_1^\beta, t_2 + \Delta t_2^\beta)] \leq (\Delta t_1^\beta + \Delta t_2^\beta)/2$ (superscript β indicates that Δt intervals are related to the **broken** state lifetime). Consequently, even if physico-chemical healing processes are longer the larger the scale is, the process of healing by geometrical blocking (non cooperative behaviors at smaller scales) can be more rapid for larger fractures. This is due to the increase of possible blockings ("*barriers*") at every smaller scale.

(iv) Suppose C is in the state **broken**. It undergoes, at time t, the transition **broken** $\rightarrow$ **moving** if it becomes "virtually" **moving** at time t, or, if at time $t - \Delta T^k$, one of its solid neighbors in $\Lambda_k(\Lambda_{k+1}(C))$ lying in the main direction which respect to C started **moving** (intra-scale propagation, already mentioned in section 2.3 for the 0 scale).

Keep in mind that the inverse cascade of rupture is instantaneous according to the S.O.F.T. rule. Consequently, a transition at the lowest level could correspond to a similar transition at higher levels. This does not mean that the rupture process itself is instantaneous because this process is in fact made of all the ruptures at lower levels which occured before this transition (intra-scale propagation and S.O.F.T. rule with memory).

2.5 The direct cascade of stress redistribution

We detail here the source of the stress heterogeneity. As we saw in the previous part, the small scale dynamics depends on the local stress in elementary cells C_i^0, $i \in \{1, 2, ..., \mathcal{R}^{K-k}\}^D$. This local stress is changed on the one hand by the external large scale loading process, and on the other hand by the internal stress redistribution following the seismic events (varying with time):

$$\frac{d\sigma(C_i^0, t)}{dt} = E + I_i(t), \tag{14}$$

where E (supposed to be constant) and $I_i(t)$ are respectively the external loading rate and the internal stress redistribution rate. A seismic event is a cell in the moving state (see however sec. 3.2) . For a cell C_j^k of level k we denote by $T^s(C_j^k)$ and $T^b(C_j^k)$ the sets of time points τ^s and τ^b when it respectively starts to move from a solid and a broken state. For the sake of simplicity we suppose that the stress is redistributed uniformly in time during the event. Therefore, we write $I_i(t)$ as follows

$$I_i(t) = I_i^s(t) + I_i^b(t) \tag{15}$$

$$I_i^s(t) = \sum_{k=0}^{K} \sum_{C_j^k} \sum_{\tau \in T^s(C_j^k)} \xi_{[\tau, \tau+\Delta T^k]}(\tau) \frac{\Delta^s \sigma_{i,j}^k}{\Delta T^k}, \tag{16}$$

$$I_i^b(t) = \sum_{k=0}^{K} \sum_{C_j^k} \sum_{\tau \in T^b(C_j^k)} \xi_{[\tau, \tau+\Delta T^k]}(\tau) \frac{\Delta^b \sigma_{i,j}^k}{\Delta T^k}, \tag{17}$$

with,

$$\xi([\tau, \tau + \Delta T^k]) = \begin{cases} 1 & t \in [\tau, \tau + \Delta T^k] \\ 0 & \text{else} \end{cases}.$$

Thus $\Delta^s \sigma_{i,j}^k$ and $\Delta^b \sigma_{i,j}^k$ are the internally redistributed amounts of stress, during time ΔT^k, into the cell C_i^0 of the elementary level when a cell C_j^k has moved respectively from a solid or a broken state. For each transition through the moving state, three contributions are taken into account. Suppressing the indices ^{s} and ^{b} we have

$$\Delta \sigma_{i,j}^k = \Delta \sigma_{loc;i,j}^k + \Delta \sigma_{red;i,j}^k + \Delta \sigma_{unif;i,j}^k, \tag{18}$$

where $\Delta\sigma_{loc}$, $\Delta\sigma_{red}$, $\Delta\sigma_{unif}$ are respectively the local stress drop, the redistribution of stress from neighbour cells, and the uniform stress drop.

First, if a cell $C = C_j^0$ at the elementary level moves, it undergoes a local stress drop which we suppose constant. This local stress drop does not happen for moving cells at higher levels and thus

$$\Delta \sigma_{loc;i,j}^k = -\sigma_{loc} \delta_{ij} \delta_{k0} \tag{19}$$

Second, if cells at higher level move, they induce a stress redistribution in adjacent cells. To model this stress redistribution we introduce for each scale k a mask F_l^k, $l \in \{-1, 0, +1\}^D$ which, for each event, determines the change of local stress in a neighborhood of the cell where the event took place.

For simplicity we only consider the next and nearest next neighbors. Moreover, we suppose that all the redistribution masks are obtained via a scaling of the mask at the smallest scale F^0. More precisely, if an event takes place in a cell C_j^k of level k, the stress in the elementary cell C_i^0 changes according to the following formula

$$\Delta\sigma^k_{red;i,j} = \begin{cases} F^k_l, & \text{if } C_i^0 \in \Lambda_0(C^k_{j+l}), l \in \{-1,0,+1\}^{\mathcal{D}} \\ 0 & \text{else} \end{cases} \tag{20}$$

The mask F_l^k is derived from F_l^0 according to the rule

$$F_l^k = \lambda \mathcal{R}^{\theta k} F_l^0 \tag{21}$$

with some parameters θ and λ. The boundary is treated by 0-extension.

[Figure 4 about here.]

For a typical example in two dimensions, see Figure 4 where we approximate in a discrete and abstract way the actual observed redistribution patterns (Okada 1985, 1992). Four parameters are used to define the mask F^0 in 2 dimensions. Here, we simply consider that there is a relative increase of the shear stress along the main direction (A_0, A_1 on Fig. 4) coupled with a relative decrease in the other direction (A_2 on Fig. 4); these relative variations represent a few percents of the local shear stress. Note that, with these definitions, an event of scale k affects the stress in all the smallest scale cells located in a neighborhood of C_j^k that grows proportionally to $l(k)$. As said in section 2.4, an event at the elementary scale may instantaneously produce larger scale events through the inverse cascade: the stress redistribution corresponding to these events generates a large heterogeneity in the stress field through the presently discussed direct cascade. This is one of the key points of the model: multiscale interactions govern the seismogenic process.

Third, an event at scale k is supposed to produce a total global stress drop $\Delta\sigma^k_{glob}$, which we will specify below. In order to respect this constraint, we add, in the case of an event at scale k, to every cell of the elementary level an uniform stress change :

$$\Delta\sigma^k_{unif;i,j} = \Delta\sigma^k_{unif} \quad \text{such that} \sum_i \Delta\sigma^k_{i,j} = \Delta\sigma^k_{glob}, \quad \forall j \tag{22}$$

Let us detail how we calculate the global stress drop, $\Delta\sigma_{glob}$. Kostrov (1974) has suggested a formula generalizing Brune's (1968) one to the case of a seismic process taking place in a volume, V. Each event of seismic moment M_0 is associated with a negative variation of the average strain, $\Delta\varepsilon_a$,

$$\Delta\varepsilon_a = -\frac{M_0}{2\mu V}. \tag{23}$$

where μ is the shear modulus. The corresponding change of the average stress, $\Delta\sigma_a$, is

$$\Delta\sigma_a = \mu\Delta\varepsilon_a = -\frac{M_0}{2V}. \tag{24}$$

In our hierarchical system, the seismic moment, $M_0(k)$, of an event of level k is given by

$$M_0(k) = \mu S(k) u(k), \tag{25}$$

where $u(k)$ is the displacement caused by the event and $S(k)$ the fault surface area. The displacement is proportional to the linear size of the corresponding moving cell ($u(k) \sim \mathcal{R}^k$), while the surface is the product of the length $l(k)$ of the cell by its height $h(k) \sim l(k)$: $S(k) \sim \mathcal{R}^{2k}$. It follows that

$$M_0(k) = \mu_1 \mathcal{R}^{3(k-\mathcal{K})}, \tag{26}$$

where $\mu_1 \sim \mu l^2(\mathcal{K}) u(\mathcal{K})$ is a constant. From Eqs. 24 to 26, it comes out that the global stress drop, $\Delta\sigma_{glob}$, due to an event of level k writes

$$\Delta\sigma_{glob}(k) = -\mu_2 \mathcal{R}^{3(k-\mathcal{K})}, \tag{27}$$

where $\mu_2 \sim 0.5\mu l^{-1}(\mathcal{K}) u(\mathcal{K})$ (we assume $V \sim l^3(\mathcal{K})$). From eq. 18 and 22, we deduce the uniform stress drop which is redistributed in the whole domain.

3 A "FRICTION" MODEL AND A "FRACTURATION" MODEL

The general model described above has a very complex behaviour, and no large range of parameters values has yet been explored. Therefore, in the present paper, we expose two submodels which have been explored in some detail and constitute the two first steps of a complete numerical simulation which will be exposed in a future work. Considering the two submodels separately is a preliminary approach to understand the origin of the different characteristics of the general model. We study here two distinct ranges of parameters which correspond on the one hand to a "fracturation" model and on the other hand to a "friction" model. They do not describe the faulting mechanism at the same time scale; they are in fact complementary submodels of the more complete one which corresponds to the theoretical formalism exposed above (section 2). For the sake of simplicity and saving computation time, we consider in the following $D = 2$. If we conserved our anisotropic S.O.F.T. rule (the critical configuration is an alignment along only one particular direction) and our schematic stress redistribution mechanism which introduces again anisotropy, a three dimensional approach would not constitute a major change in principle (see sec. 2, Figures 3 and 4), even if, in the classical renormalisation techniques, the dimensionality of the system exerts an important control on its behaviour. Nevertheless, a full realistic 3D approach would not be so simple to implement, given that faults may occur in different orientations, and that the addition of gravitational effects may be significant.

[Table 1 about here.]

3.1 A "friction" model

This model corresponds to a completly fractured fault zone. To study this "friction" process starting from our general model, we simply take (c.f. Tab. 1 **C**) a completly broken initial state (all the cells, $\forall k$, are broken) without healing process ($\beta = 0$).

Let us give the basic properties of this simpler model within the framework of the general one. We are left with two states, **broken** and **moving**. The transition $b \rightarrow m$ at the elementary level is determined by a stochastic random process (eq. 12) while at higher scales ($k > 0$) it is determined by the S.O.F.T. rule applied to the cells of the lower level ($k - 1$). The transition $m \rightarrow b$ is deterministic at all scales, k; a cell stops moving a time ΔT^k after it started moving at time t. If during this time span $(t, t + \Delta T^k)$, the **moving** cell becomes virtually **moving** again (because at smaller scale a SOFT configuration occurs) it still will stop at $t + \Delta T^k$.

Before generating a seismic catalog (time, magnitude, location), let us precise what we call, in this model, an earthquake, its magnitude, its nucleation, time and location.

We define the nucleation time-point and its position in a recursive way. If a cell C at level k starts **moving**, it either participates in the nucleation of an event of larger scale $k + 1$, or it represents the endpoint of a "friction" cascade. It is the endpoint in a "friction" cascade, if, during its moving time ΔT^k, the cell $\Lambda_{k+1}(C)$ does not start moving. Note that $\Lambda_{k+1}(C)$ may already be **moving**, in which case automatically the event occuring at C is the endpoint of a friction cascade. We say that a cell C of level k participates in the nucleation of an event, if, during ΔT^k, its moving time, the cell $\Lambda_{k+1}(C)$ undergoes a transition to the moving state as well. This motion, however, may have been initiated by some other cell in $\Lambda_k(\Lambda_{k+1}(C))$. We now define the nucleation location and time at scale k of a larger event of scale $k + 1$: it is the position of the first cell in $\Lambda_k(\Lambda_{k+1}(C))$, lying in the main direction with respect to C, which started to move and the time when it started to move. This defines in a recursive way the nucleation location and time of any event at the smallest scale. In case a cell C^k at level k is the endpoint of a cascade (see above), we report in the catalog its nucleation time and location at the elementary scale through the recursive scheme described above; we say that an earthquake of level k was initiated at this time point and location.

An earthquake of level k is associated with the **moving** state of a cell of level k. This event has to be given a magnitude, completely defined by its level k. This magnitude, $M(k)$, can be obtained from eq. 26 using the relationship $\log(M_0(k)) = 1.5M(k) + const$, or directly from $M(k) = \log(S(k)) + const$ (Kanamori & Anderson 1975). In both cases, we obtain

$$M(k) = 2k \log(\mathcal{R}) + const. \tag{28}$$

Let us insist on some important peculiar characteristics of the model. First, we can describe the

nucleation phase, the coseismic phase and the stopping phase of an earthquake (c.f. section 4.3) as a cascade model (Ellsworth & Beroza 1995). Second, the propagation of the moving state (due to stress redistribution) at the elementary level can proceed at different rates and could be associated or not with a higher scale event. Let us illustrate different situations in the one dimensional case of figure 5 (N and t_i are defined in the caption).

(i) $t_N - t_1 \gg \Delta T^K$: the propagation proceeds very slowly, there is not highest level event and this corresponds to the seismicity along creeping faults (we now call creep this behaviour).

(ii) $t_N - t_1 > \Delta T^K$: the propagation proceeds slower than the rupture, there is not highest level event and this corresponds to the seismicity during a slow earthquake.

(iii) $t_N - t_1 \leq \Delta T^K$: the propagation is very rapid, there is an event of the highest scale with a stick-slip mechanism.

[Figure 5 about here.]

3.2 A "fracturation" model

As in our previous approach (Allègre et al. 1995, 1998), this model corresponds to a weakly fractured fault zone where the healing process is effective at the lowest scale ($\beta \neq 0$). This process generates a hierarchical geometric blocking at higher scales. To particularize the "fracturation" submodel from the general one, we simply adopt (c.f. Tab. 1 **B**) an instantaneous propagation of rupture ($\Delta T^k \to 0, \forall k$) and a continuous shear stress dissipation by friction. Thus we end up with a two states model, solid and mobil-broken. To incorporate the dissipation by friction, we let k_b go to infinity in eq. 12, in such a way that, as soon as the stress reaches the critical threshold value σ_b, the cell undergoes a transition $b \to m$ and stays moving for an infinitesimally small time ΔT^k before it becomes broken again. Note that the transitions $b \to m \to b$ are not visible in our condensed two states (solid and mobil-broken) "fracturation" model. During the infinitesimal time ΔT^k, the excess of stress with respect to σ_b is evacuated from the system, eliminated by the "friction" process.

Let us recall, in the framework of the general model, the basic characteristics of this simpler model. We have two states, solid and mobil-broken (we now use broken for this double state). The transition $s \to b$ at the elementary level is determined by a stochastic random process (eq. 4 to 9) while at higher scales it is determined by the S.O.F.T. rule applied to the broken cells of the lower level. The transition $b \to s$ is also determined by the S.O.F.T. rule: a cell which is not in the broken state is in the solid one.

To generate a seismic catalog (time, magnitude, location), let us define precisely what we call, in this model, an earthquake, its magnitude, its nucleation time and location. An earthquake is here

associated with the $s \rightarrow b$ transition. Since the rupture instantaneously propagates through the higher levels, transition $s \rightarrow b$ at the elementary scale is called an "hypocenter"; this is indeed the nucleation of the fracture which can go up the scales, thanks to an inverse cascade. All these nucleations are noted in the catalogue. Of course, there is no earthquake duration in this case. For a given event, the magnitude is given by eq. 28, as in the "friction" model.

4 RESULTS OF NUMERICAL SIMULATIONS

As said above, we study two distinct ranges of parameters which correspond on the one hand to a "friction" model and on the other hand to a "fracturation" model. We are interested in the most general properties of the events sequences obtained from the numerical simulations; these are the magnitude-frequency relationship, the temporal variation of the number of foreshocks and aftershocks per unit of time, the periodicity of strong events. For both models, in a wide range of parameters values, events (earthquakes) sequences perfectly obey both Gutenberg-Richter and modified Omori laws.

Let us first discuss the parameters kept constant in each model (c.f. Tab. 1**A**). $\mathcal{R}$ is taken equal to 2; a larger renormalization factor would only provide a more realistic magnitude-k relationship (eq. 28) and an increase of the number of foreshocks and aftershocks (Allègre et al. 1998). The latter statement is still valid when considering the effect of an increase of the number of scales, $\mathcal{K}$ (see Fig. 12). A small number of scales is not a big drawback because of the self-similar behaviour at all scales except the elementary one ($\mathcal{K} = 0$); note that the typical length of an elementary cell is related to this number of scales. All the parameters concerning the stress field (σ_b, σ_s, $\Delta\sigma_{loc}$, μ_2) are of the order of magnitude of the observed ones. Parameters related to eqs. 9, 12 (δ_s, δ_b, k_s, k_b) are arbitrarily chosen.

4.1 Method of analysis

We obtain as a result numerical catalogs of events (see above). These catalogs contain the times of events, the "hypocentre" coordinates, the hierarchical level reached by the event and the corresponding magnitude (c.f. eq. 28). We also follow the evolution of the total transition rate at the lowest scale, of the average shear stress, and of the heterogeneity of the stress field.

Making use of eq. 28 for the conversion from hierarchical level to magnitude, we estimate the b-value of the Gutenberg-Richter relationship through the formula

$$b = \frac{1}{2\log(\mathcal{R})}\log\left(1 + \frac{1}{\overline{k} - k_m}\right) \tag{29}$$

where $\overline{k}$ and k_m are respectively the average and the minimum hierarchical levels in the considered set or sub-set of events. This formula is the maximum likelihood estimate of the b-value in the case of a non-limited range of discrete magnitudes with integer values (Molchan, Kronrod & Panza 1997;

Kulldorf 1961). The limitation of the magnitude of events by the highest scale in our model is not important for the comparative analysis. The magnitude band of the model is derived from the number of hierarchical levels through eq. 28, and the maximum magnitude is fixed by the characteristic length of the highest level.

For the temporal analysis of foreshocks and aftershocks, we used the program AFT developed by Utsu, Ogata & Matsu'ura (1995). This program is available in the IASPEI Program library (Lee 1997). We estimated the parameters of two different models of the aftershocks decay (or foreshocks increase): the modified Omori law (Utsu, Ogata & Matsu'ura 1995) and its modification known as Otsuka model (Otsuka 1985). The modified Omori model assumes a power-law decay:

$$f(t) = \frac{A}{(t+c)^p} \tag{30}$$

$f(t)$ is the number of events per time unit, t the time from the main shock, p the Omori exponent and c a shifting parameter. In Otsuka model the long tail of the power-law is reduced by introducing an exponential with a characteristic time T:

$$f(t) = \frac{A}{(t+c)^p} \exp(-\frac{t}{T}) \tag{31}$$

Parameters of eqs. 30, 31 are computed in the program AFT using the maximum likelihood method and the Davidon-Fletcher-Powel optimization procedure (Utsu, Ogata & Matsu'ura 1995). Unfortunately, this program does not work with sequences containing more than 5000 events. We then developed our own code which can be applied to unlimited sequences.

4.2 Identification of the events

Let ΔT_{aft} be a time span which will be defined below. Main shocks and aftershocks are identified in the following way:

if an event of level k at time t is preceded by only lower level events in $[t - \Delta T_{aft}, t]$, it is a main shock with precursors.

if an event of level k at time t is not preceded by an event during $[t - \Delta T_{aft}, t]$, it is a main shock without precursor.

if an event of level k at time t is preceded in $[t - \Delta T_{aft}, t]$ by an event of level k which is not an aftershock, it belongs to a swarm of level k.

if an event of level k at time t is preceded by a larger level event during $[t - \Delta T_{aft}, t]$, it is an aftershock.

ΔT_{aft} is chosen (by trial and error) in such a way that about 90% of the aftershocks of a main shock (identified as said above) which occured at time t are contained in $[t; t + \Delta T_{aft}]$. ΔT_{aft} depends

essentially on the parameters of the mask. These rules are somewhat arbitrary, but we have observed that the results do not depend much on ΔT_{aft} if this value is few orders of magnitude less than the average time interval between two main shocks.

4.3 Numerical results of the "friction" model

In the "friction model" $\pi(t)$ is the total transition rate $b \rightarrow m$ at the elementary scale and we will interpret in terms of foreshocks-main shock-aftershocks the short time period from the nucleation phase to the stopping phase of a given event.

[Figure 6 about here.]

"Friction" model with immediate load We suppose a very small loading rate which will not change significantly the system during the characteristic duration of a foreshocks-main shock-aftershocks sequence. Starting from an homogeneous state, the system can have been loaded up to the critical stress value ($\mathcal{R}^{DK}\sigma_b \; bars$) by the stress ($E$) applied to the boundary of the domain by plate tectonics. According to eq. 12, this is indeed possible in the case of a homogeneous system, because nothing occurs as long as $\sigma_i < \sigma_b$. We can as well take as the initial ($t = 0$) configuration $\sigma_i = \sigma_a = \sigma_b \; \forall i$. A first transition $b \rightarrow m$ is randomly chosen in the volume. This first nucleation is enough to obtain, without additional loading, an increase of the foreshocks activity, a main shock and aftershocks. Let us explain this behaviour. The perturbation of the stress field around the first moving cell ($\Delta\sigma_{red}$) is larger than the uniform stress change ($\Delta\sigma_{unif}$) calculated from the global stress change ($\Delta\sigma_{glob}$). Consequently, at the elementary level, the rate of transitions $b \rightarrow m$ ($\pi(t)$) increases; the heterogeneity of the stress field increases after each event at the elementary level, and so on. The process is auto-accelerated, events at higher level occur and, finally, a strong event may occur. This is the time of the largest stress field heterogeneity. A strong event (or strong events) significantly unloads the whole system. This starts the cascading of the aftershocks which unload the areas of high stress and decreases the average stress (σ_a). The value of $\pi(t)$ decreases rapidly at the beginning, but this decreasing is then slowing down due to the decreasing of σ_a.

The general results are as follows. First, in a very large range of model parameters values, we obtain sequences with an increasing frequency of foreshocks preceding a main shock or several strong events (swarm) followed by a sequence of aftershocks with a decreasing density. Second, the temporal decay of the number of aftershocks per time unit obeys in general the modified Omori law, in many cases perfectly. The value of the power exponent is usually around 1.5. Third, the events sizes distribution follows very well the Gutenberg-Richter law; b-values vary in the range 0.5-5.0 depending upon the different parameters values sets, and vary also with time, for given parameters, during

the foreshocks-main shock-aftershocks sequence. Fourth, foreshocks also often follow a power law increase.

We now present in more detail the behaviour of the system for different values of the parameters for and around the ones reported in Tab 1 **A** and **C**.

[Figure 7 about here.]

Results corresponding to the parameters values set of Tab 1 **A** and **C** (the reference sequence) are shown on Fig. 6 versus both linear (Fig. 6(a)) and logarithmic (Fig. 6(b)) time scales, reckoned from the time of the first nucleation (see above). On each subfigure the first graph shows the level of the events, the second one shows the total transition rate $b \rightarrow m$ at the elementary scale, the third one represents the evolution of the average global stress, the fourth one the evolution of the standard deviation of the stress distribution for levels 0 and 1, and the last one shows the density d of currently moving cells at the elementary level; note that at the moment of the main shock this number is less than at the time of the strong foreshocks. Both values of d are much less than the critical density value (0.618) of the corresponding integral S.O.F.T. model. This "reference" sequence summarizes the typical behaviour of the "friction" model. The main shock is preceded by a short sequence of foreshocks. With the logarithmic time scale we clearly see the temporal clustering of events: strong foreshocks are themselves preceded by foreshocks and have their own aftershocks. The main shock has a rather long sequence of aftershocks. Fig. 7 shows that the temporal aftershocks activity decay with time obeys very well the modified Omori law. Fig. 7(a) shows in a logarithmic time scale the cumulated number of aftershocks compared with the theoretical curve (eq. 30) for the values $p = 1.52$, $c = 203$ given by the maximum likelihood estimation. Fig. 7(b) shows the cumulated number of aftershocks versus the number given by eq. 30.

[Figure 8 about here.]

The events sizes statistics follows the Gutenberg-Richter law. Fig. 8 shows separately the magnitude-frequency curves for foreshocks and aftershocks with b-values respectively equal to 1.43 and 2.06. The slope break for the magnitude-frequency curve for all events ($b = 1.85$) at $k = \mathcal{K} - 1$ is a finite size effect (only one highest scale event is recorded in the analysed sequence). Fig. 9 shows the temporal variation of the b-value, estimated at time t by eq. 29 using the last 200 events before t. We see that the b-value has a minimum just before the main shock as this is often observed for large earthquakes (Smith 1981), even if not systematically.

[Figure 9 about here.]

Such an observation was discussed in Main et al. (1990) and has been observed in controlled tests by Sammonds, Meredith & Main (1992). These authors call for a (short or prolonged) strain-softening mechanism. Similarly, in our approach this minimum of the b-value stems from the growth and the coalescence of old cracks, two major ingredients of the strain-softening mechanism. Coalescence at all scales (self-organization) is an intrinsic property of the S.O.F.T. rule, and no particular mechanism (e.g. pore-fluid pressure) is implicitly modeled; this is an advantage (and may be a drawback) of our model.

We have then varied the parameters around the values of the reference sequence and found that the behaviour is unexpectedelly insensitive to the change of most parameters. Except for marginal cases with no strong events or too short sequences of aftershocks, the system provides almost perfectly both a Gutenberg-Richter distribution of events sizes (with b-values for foreshocks smaller than for aftershocks) and an Omori law of the temporal aftershocks decay (see discussion, sec. 5). The model appears to be the most sensitive to changes of the parameter k_b which has the dimension of the inverse of a time.

[Figure 10 about here.]

The foreshocks-main shock-aftershocks sequence can be more complex than in the reference case. Fig. 10(a) shows a main shock followed by a short sequence of aftershocks. Afterwards, during a rather long time interval, no event occurs, and, after this "quiet" period, the aftershocks sequence starts again to finally relax the system. Fig. 10(b) shows the case of several main shocks (swarm). The case without strong event corresponds to creep (see Fig. 13, this case will be met in a next paragraph).

[Figure 11 about here.]

An interesting log-periodic variation of the aftershocks frequency is superimposed on the trend (Fig. 11(a)). On Fig. 11(b) these log-periodic oscillations are seen around the theoretical straight line. This reflects the temporal distribution of the major (leading) aftershocks which are themselves followed by a sub-sequence of aftershocks (Correig, Urquizú & Vila 1997). In some cases we obtained a similar behaviour for the foreshocks sequences, but with only 2-4 oscillations (Fig. 6). Note that an attempt to rigorously test this pattern in earthquakes catalogs (Gross & Rundle 1998) produced a negative result. In the same way, it is not observed in all our numerical simulations; we have not yet been able to define the range of parameters where this pattern clearly occurs.

[Figure 12 about here.]

Let us now see how the model behaviour depends on the number of levels $\mathcal{K}$; if the scaling works properly, this dependence must be weak. Figures 12(a1), (b1), (c1) show sequences obtained with 5,

6 and 7 levels ($\mathcal{K} = 4, 5, 6$) retaining only the five highest levels. All the other parameters of the model are kept the same; this corresponds to systems with different spatial sizes but the same physical parameters. The sequences corresponding to the different $\mathcal{K}$ obey almost perfectly the Gutenberg-Richter law of events sizes distribution and the Omori law of aftershocks decay. The most important difference is the duration of the power-law behaviour of the aftershocks sequence as estimated by the parameter T in the Otsuka formula (eq. 31). It decreases with the number of levels (Figures 12 : (a2), (b2), (c2)). This decrease of T is due to the fact that the direct cascade redistributes more stress at the lowest level for a higher value of $\mathcal{K}$. A more sophisticated rule including a redistribution of stress at all scales would increase the value of T (and make the difference of behaviour in function of $\mathcal{K}$ weaker).

[Figure 13 about here.]

"Friction" model with constant load What happens after the main shock and aftershocks have passed? How does the external loading start new events? Is it possible to obtain an analogue of the seismic cycle? We understand the term "seismic cycle" as the recurence time (quasi-periodic or almost stochastic) of strong earthquakes, generally preceded by a growing seismic activity (foreshocks), followed by sequences of aftershocks and with a relatively aseismic behavior between foreshocks-main shock- aftershocks sequences (Fedotov (1965) ; see also the detailed review with a large bibliography in Scholz (1990)). In the model described above no strong events occur again; all the received energy is dissipated in small events; in this "weak" system (low value of E) the dissipation keeps the average stress below the critical value (Fig. 13(a)). In the case of a "strong" system (strong value of E) with a high rate of external loading, the average stress can be larger than the critical value (Fig. 13(b)). Both cases can be interpreted as creep. But, in another "friction" submodel derived from the present one through only a small modification, we do obtain a seismic cycle; we suppose that the local stress heterogeneity is slowly decreasing with time due to some kind of "diffusion" process, at a rate assymptotically proportional to the square root of time:

$$\sigma(C, t + \Delta t) = \sigma_a(t) + \frac{\nu}{\sqrt{\nu^2 + \Delta t \Upsilon}}(\sigma(C, t) - \sigma_a(t)) \tag{32}$$

where ν is a dimensionless constant parameter, $\sigma(C, t)$ the local shear stress in the cell C, $\sigma_a(t)$ the average stress, and Υ a reduced diffusion coefficient (s^{-1}). Fig. 14 shows the numerical results for the set of parameters of the reference sequence except for $E = 10^{-4}\ bars/s$ and $\Upsilon = 10^{-4} s^{-1}$, $\nu = 1$. Each peak corresponds to a foreshocks - main shock - aftershocks sequence which has the same statistical behaviour as the reference sequence.

[Figure 14 about here.]

4.4 Numerical results of the "fracturation" model

In the "fracturation" model, $\pi(t)$ is the total transition rate $s \rightarrow b$ and $b \rightarrow s$ at the elementary level. At higher scales, the $s \rightarrow b$ and $b \rightarrow s$ transitions are respectively associated with a seismic event or a geometric blocking. Given a slow physico-chemical healing at the lowest scale, we study the seismicity over long time periods. The stress balance is between the external input and both discontinuous "fracturation" events ($s \rightarrow b$ transition) and continuous "friction" (broken cells C lose the excess stress $\sigma(C) - \sigma_b$ they receive from outside (E) or from internal redistribution). We now present some typical earthquakes sequences and describe the statistical behaviour of the model for different values of the parameters. The unit of time in all the figures is $10^2 s$. In captions we indicate the differences between the Tab. 1 **A** and **B** parameters values and the ones of the current numerical experiment.

4.4.1 General properties of a sequence (a realization for a given set of parameters)

[Figure 15 about here.]

Temporal distribution of earthquakes: Fig. 15 shows a typical sequence on a short time period (a time interval containing 2 events of the highest level). We can observe several main shocks of different amplitudes: (b2) and (b3) of level 6, (b1) of level 5, (c) and (d) of level 4, (e) of level 3; depending on their geometrical distribution, the same number of broken cells can give events of different levels (compare (a1) and (a3)). Comparing (a3) with (a2) shows that the average stress is correlated with the number of solid cells at the elementary level. Some main shocks have precursors ((b3),(c1),(c2)), while some other ones have not ((b1),(b2),(e)). These precursors can be themselves followed by aftershocks ((b3),(c1)). Each main shock has its own aftershocks sequence. The last main shock on the picture (b3) has a large aftershock followed by a sub-sequence of aftershocks; this large energetic release reduces the duration of the main aftershocks sequence. For lower level main shocks ($k < K - 1 = 5$), due to the small number of levels ($K = 6$) and the value of the scaling parameter θ (eq. 21), one observes on the one hand a longer duration of the aftershocks sequence, and on the other hand a smaller number of them. This long duration of the aftershocks sequence is not observed for higher level main shocks ($k > 4$); it is a consequence of the direct cascade mechanism which redistributes all the stress drop from higher levels events directly onto the elementary level. The evolution of the average shear stress is self similar ((a2),(c2), (d2) and (e2) have the same behaviour but on different time scales). The interseismic period between the two main shocks of the highest level ((b2) and (b3)) is 600 years, the time lengths of figure (e1) is 4 years and the time length of figure b(1) and (b2) are 45 days. Note that the global stress drop associated with (b3) is due to a temporal seismic migration: a level 4 event triggers a level 5 event which in turn triggers a level 6 event. Finally, one clearly sees on figure 15 the temporal

clustering of the events. The spatial clustering is also present: aftershocks (main shocks) occur in the neighborood of the main shock (foreshock), where the redistribution of stress is positive. Given our two dimensional system and the anisotropy of the critical S.O.F.T. rule, we postpone the study of the spatial distribution of our events.

[Figure 16 about here.]

Aftershocks: Fig. 16 shows a typical aftershocks sequence (during 2 months) without large events among them (this explains the low number of aftershocks because there is no secondary sequence of aftershocks). Rule (30) is respected (Fig. 16(a4) and Fig. 16(a5)), and this is the case for a large range of parameters (see below). Let us explain the aftershocks generation mechanism. The redistribution of stress rapidly increases the transition rate $s \rightarrow b$ according to eq. 9. The increase of the transition rate $b \rightarrow s$ is much slower because during the aftershocks sequence this rate is inversly proportional to the number of solid cells (Fig. 16(a3)); in other words, just after the main shock, the "fracturation" process is more efficient than the healing process. Later on, both local and global stress drops (Fig. 16(a1) and 16(a2)) favor the decrease of the transition rate $s \rightarrow b$ while each fracturation increases the transition rate $b \rightarrow s$. This balance is reached rapidly just after the main shock and more slowly later on, in agreement with the modified Omori law. The main cause of this typical $(1/(t+c)^p)$ behaviour is the heterogeneity of the stress field (Fig. 17(b)); in the case an event perturbs a medium where the stress field is completely homogeneous, the decrease of the aftershocks frequency is exponential (Fig. 17(a)).

[Figure 17 about here.]

[Figure 18 about here.]

Foreshocks: Foreshocks are here obviously present: the fracturation mechanism cannot directly reach the highest level and the organization of a fracture at a given scale requires lower scale fractures. Nevertheless, due to the history of the fault zone, their time distribution is very complex. For studying only the distribution of foreshocks we select in our catalogs examples where earthquakes of lower amplitude precede a main shock, and we eliminate the aftershocks (i.e. all the lower level events occuring after the higher level one). If the medium is weakly fractured (high value of β) and the stress field is homogeneous ($\sigma_a = \sigma_s$), the foreshocks activity satisfies the modified Omori law (with $t \rightarrow -t$; the typical exponent is called q instead of p (Fig. 18(a)). If the medium is not fractured (high value of β) and the stress field is heterogeneous, the foreshocks activity respects the modified Omori law ($t \rightarrow -t$) with a lower value of q (Fig. 18(b)). If the medium is fractured (low value of β) and the stress field is heterogeneous, a main shock occurs without foreshocks and it is very difficult to isolate the foreshocks from the background seismicity.

[Figure 19 about here.]

Magnitude-frequency relation Fig. 19 shows the magnitude-frequency relationship for a typical sequence on a very long time period (0.3 My). The slope of the magnitude-frequency relationship for the main shocks is smaller than the slope of the magnitude-frequency relationship for all the events, which is in turn smaller than the slope corresponding to the aftershocks sequences for different levels of main shocks. The magnitude-frequency relationships for aftershocks sequences of main shocks with different magnitudes do not have significantly different slopes. The b-value could be easily made closer to 1 with a more appropriate renormalisation factor (c.f. eqs. 28 and 29). The slope break between levels $\mathcal{K}$ and $\mathcal{K}-1$ is an effect of the finite domain.

4.4.2 Statistic properties on a set of sequences

In the following we select main shocks of level $k \geq 4$ (i.e. 4,5,6) and ΔT_{aft} is adjusted for each sequence.

[Figure 20 about here.]

Aftershocks: The behaviour of the aftershocks sequence essentially depends on the sharpness of the $s \rightarrow b$ transition (δ_s in eq. 9). As showed above, the aftershocks sequence is due to the increase of the local shear stress resulting from the direct cascade of stress redistribution. Each aftershock modifies in its turn the local shear stress in its neighborood; this perturbation decreases with the magnitude following the scale dependent law of parameter θ (eq. 21). Figure 20 shows that the power law decrease $(1/(t+c)^p)$ is still respected if $\delta_s > 2$; below this threshold value, $c/\Delta T_{aft}$ becomes too large: the global and local stress drops due to each aftershock are not large enough to decrease the $s \rightarrow b$ transition frequency, and a constant rate of aftershocks results. We observe that the p value decreases if the value of δ_s increases (Fig. 20(a)). The number of aftershocks and the b-value (Fig. 20(c) and (d)) do not depend on δ_s.

[Figure 21 about here.]

Influence of the stress redistribution: The external loading rate E and the healing rate β are physical parameters which obviously compete in the process. We have studied the variation of different outputs of the model in function of the density of fractures for different values of $E \in [10^{-9}; 10^{-4}]$ and $\beta \in [10^{-11}; 10^{-5}]$. In figures 21, 22, 23 each point results from a numerical simulation over a sequence of long duration ΔT ($\Delta T = 10^6 \Delta T_{aft}$).

Fig. 21(a) shows the b-value of the frequency-magnitude distribution versus the density of broken cells of the lowest level (in fact the density average over the whole sequence duration). We observe a

minimum at $d \sim 0.3$ and a plateau for a large range of $d \in [0.4; 0.7]$. The theoretical curve obtained by the integral approach has a minimum at $d_c = 0.618$, the critical value of this approach (see caption Fig. 21). This difference in behaviour is due to the stress redistribution which organizes the "fracturation" process in a weakly fractured medium: the mask increases the stress in the neighboring cells along the main direction of the cracked cells. Thus the fault zone can generate high magnitude events even if the density of cracks is less than the critical value.

Fig. 21(b) shows the ratio $f = w_1/w_2$ between the total stress eliminated by the "fracturation" process (through the global stress drop, $w_1 = \sum_k \sum_{events} \mu_2 \mathcal{R}^{3(k-K)}$, eq. 26) and the total stress eliminated by the "friction" process (see 3.2, $w_2 = E\Delta T - w_1$), versus the density of broken cells. The theoretical curve obtained from the integral approach has a maximum at the critical value of this approach. For $d > d_c$ the two behaviours are similar; below this value, the "'fracturation" process is more efficient for the present model with stress redistribution; the maximum value of f is reached at the value of d giving the minimum of the b-value (Fig. 21(a)).

[Figure 22 about here.]

The stress input during the broken lifetime $(1/\beta)$**:** Let us now study the behaviour of our system versus E/β which has the dimension of a stress. Figure 22 shows that some of the system main characteristics are largely controlled by this single parameter. The "fracturation process" (fig. 22(a)) is negligible if $E/\beta > 10^2$. Below this value a typical peaked behaviour is observed. We will come back to this result in section 5. The b-value versus (E/β) curve shows that b is controlled by (E/β) as long as $(E/\beta) < 10^2$ and exhibits (fig. 22(b)) a clear minimum. For high values of E/β, the number of high degree events is weak and the b-value is controlled by the healing mechanism. The critical (E/β) value for which b is minimum could be also inferred from fig. 22(c) whose different curves represent the densities of cracks versus E/β for different values of β; the convergence point corresponds to the critical density of cracks and the critical value of E/β. Note that this value, expressed in $bars$, is of the order of magnitude of the average stress (see table 1). A dimensional analysis could be investigated in a future work.

[Figure 23 about here.]

The seismic cycle: After eliminating the strong aftershocks and foreshocks, as explained previously, we noted the time intervals between two events of level $k \geq K - 1$ (i.e. 5,6). For a minimum set of 50 time intervals, we calculated Q, the ratio of the average time interval to the standard deviation of the distribution of these time intervals. Larger values of Q reflect a more periodic behaviour. On figure 23(a) we have drawn Q versus E/β for (E/β) varying only in $[10^{-3}; 10^3]$ (for lower or higher values, the high level main shocks number is too weak). A large fluctuation of Q exists, but a more

periodic behaviour is observed for lower values of E/β. On figure 23(b), the b-value s represented versus Q. An increase of the b-value is coupled with a more periodic behaviour. Such an observation is still difficult to make in real seismicity due to the short time period covered by earthquakes catalogs.

5 COMPARISON WITH EXPERIMENTAL EVIDENCE. A DISCUSSION

We are aware that even a good reproduction by a model of some regularities or empirical laws of real seismicity might not be taken for a strong evidence of the validity of this model. One of the reasons is that many of the regularities or empirical laws which have been claimed to be found in the experimental evidence are controversial (to various degrees). Only may be the Gutenberg-Richter law and the Omori law are not. But these two very general laws do not constrain the models as strongly as it could be hoped. Indeed the Gutenberg-Richter distribution is rather easy to obtain (Allègre et al. 1998). Simple toy models of self-organized criticality -such as a sand pile or a forest fire- display a power law distribution of the cluster sizes (Turcotte 1999). The Omori law appears more difficult to fit with model series. Again simple models, for example the ones which exhibit the edge of chaos dependance (Chen, Bak & Obukhov 1991), produce results which obey it. That does not make the confrontation of the model results with these two general and generally accepted empirical laws less necessary; Gutenberg-Richter and Omori laws must be observed. Let us note that obeying simultaneously both laws is signicantly more constraining than obeying either one or the other. Comparison with more controversial observed regularities or empirical laws of seismicity must be accompanied by the required caveats. And, when necessary, the subdomain of parameters for which the agreement between the model products and experimental evidence must be at least sketched (models in general and our own in particular have several adjustable parameters). In any case, confronting the model results with regularities or empirical laws observed in real seismicity -even controversial to some extent- is more efficient than confronting them with experimental evidence as a whole, without sorting. Moreover it gives the opportunity to explain why the model works the way it does.

We discussed several times the stress pattern in the model (sect. 2.5 and 3), while little is known about the seismogenic stress in nature. In fact we do not use in our reasoning any detailed knowledge of the stress field. We only call for a heterogeneous stress field which results from the mechanism of multiscale redistribution of stress described in sect. 2.5 and chosen for its simplicity (stress is relaxed in some cells, enhanced in neighbour ones, and this at all scales). What is an important aspect of the model is that the zone of influence where stress redistribution takes place (Fig. 4) grows proportional to the length of the fracture. This is consistent with much of the literature on faults growth (e.g. Main (1996)), contrarily to what happens with many S.O.C. models which do not have this property since they rely on the nearest neighbour effects at the small scale.

The above discussion bears on the comparison of the model productions with real seismicity laws (statistics on occurence time and magnitudes). Confrontation with field tectonics is another requirement. We postpone this (ambitious) objective untill we make use of the localisation properties of the model we have just mentioned in the present work (see next section).

6 CONCLUSION AND PERSPECTIVES

The new approach presented here, with a direct simulation of the stress redistribution, is an extension of the previous S.O.F.T. model. We have now built a numerical laboratory which will allows a large number of experiments characterized by different time scales, from the dynamics of the rupture ("friction" submodel) to the history of a fault zone ("fracturation" submodel). Our present modeling produces a large range of observed seismic sequences with a precise temporal (and spatial) location of the events.

The multiple scale approach coupled with the S.O.F.T. rule with memory has allowed us to incorporate the major components of the brittle fracture: healing of cracks, increase of microcracks density, rupture threshold, heterogeneity of the stress field, propagation of the fracture. Incorporating these properties in our abstract modeling gives rise to a large number of complex behaviours which can be related to the complexity of real earthquakes. The simplicity of the model is an advantage to better understand the physical origin of the complexity of the behaviours. Statistical properties of our system have been studied, even if the main goal of the present paper was more specifically to reproduce the spatio-temporal clustering of earthquakes.

We have shown that the $(1/(t+c)^p)$ behaviour of the aftershocks frequency is a direct expression of the heterogeneous stress distribution at the main shock time (see sec. 4.3 and 4.4). This conclusion is valid for both submodels since the mechanism of the stress redistribution is the same. In real earthquakes, aftershocks are present in most cases and the variation of the p value can be analysed in function of the heterogeneity of the stress distribution.

The physics of the healing (physico-chemical process or geometrical blocking) has to be taken into account in a fault zone. The ratio (E/β) between the external loading rate and the healing appears as a general control parameter. The value of this parameter discriminates between the domains of applicability of the two submodels. The foreshocks activity during the long time period preceding an earthquake indeed strongly depends on E/β. If this rate is high, an increase of seismicity is observed before the main shock, and foreshocks obviously occur; the unstable state is reached through the fracturation of the solid parts of the medium. On the contrary, with a low healing rate, the system always stays in an unstable state around a critical distribution of cracks, and the foreshocks activity is random.

The relative density and the distribution (structural heterogeneity) of the solid parts of the medium on the one hand favor the loading up of the shear stress which can be eliminated by earthquakes and on the other hand control the dimension of the largest earthquake which can occur in a fault zone.

A quasi-periodic seismic cycle is obtained in both submodels when the stress field becomes quasi-homogeneous during the loading period (interseismic phase). In the case of the "fracturation" submodel the periodic character of the seismic cycle is enhanced when b-value decreases.

There are a lot of items we intend to tackle in the future. We have to develop systematic studies of the statistical properties of our system and determine the origin of their variations. To understand the mechanism which leads to the main shock, and to decide wether this mechanism is different or not from the relaxation process, we have to study how the distribution of the stress field influences the increase of the foreshocks activity. The relative density of the main shocks with precursors has to be evaluated, and we will try to draw a phase diagram representating the different types of seismic processes: creep, swarm of small earthquakes, earthquakes with or without precursors. We will try to develop the relationship between these seismic processes and, for exemple, the parameters of the friction and fracturation laws (eqs. 9, 12) (as done here for the aftershocks frequency decay in function of δ_s). We will also pay a lot of attention to the particular case of earthquake triggering.

We will also consider a three dimensional hierarchical model with a tensorial stress field rather than a scalar one and interactions between cracks of different orientations (e.g. following Allègre & Le Mouël (1994)). It will be possible to compare our synthetic catalogs -containing both times and locations- with real data and to constrain in turn our physical parameters. This stage is of course the most important from the geophysical point of view. We have to interact with rock mechanicists to incorporate in our model more realistic ingredients for the rupture propagation and to develop a fragility criterion in a static (nucleation) or in a dynamic case (growth). It will be possible to calculate synthetic seismograms of large events taking into account the history of the rupture. It will also be important to refine the mechanism of the stress redistribution during the relative short time period following an event and its relation with the aftershocks activity and the heterogeneity of the stress field. With our mutiple scale approach we will try to answer the following questions: how an a priori heterogeneous stress field at the lowest scale can produce major ruptures accomodating the global tectonic stress field (introduced at the highest scale) and how does the system redistribute at lower scales this global tectonic stress field?

Geology is obviously heterogeneous. Introducing a three dimensional fault zone model with pre-existing geological structures is a promising perspective. In the domain of the fault zone where an event takes place, the system will not only receive a constant rate of potential elastic energy but also an unsteady rate through the interaction with the neighbor fault systems (see the multi-domains approach

in Allègre et al. (1995)). This can be done in the framework of a three dimensional rupture process where our multiple scale approach constitutes a necessary simplification.

ACKNOWLEDGMENTS

We are grateful to Ian G. Main and a anonymous referee for their constructive review. Shebalin, P. was partially supported from National Sciences Foundation Grant EAR-9804859.

REFERENCES

Aki, K., 1984, Asperities, barriers, characteristic earthquakes and strong motion prediction, *J. Geophys. Res.*, **86**, 5867–5872.

Allègre, C. J. & Le Mouël, J. L., 1994, Introduction of scaling techniques in brittle fracture of rocks, *Phys. Earth Planet. Int.*, **87**, 85–93.

Allègre, C. J., Le Mouël, J. L., Chau, H. D. & Narteau, C., 1995, Scaling organization of fracture tectonics (S.O.F.T.) and earthquake mechanism, *Phys. Earth Planet. Int.*, **92**, 215–233.

Allègre, C. J., Le Mouël, J. L. & Provost, A., 1982, Scaling rules in rock fracture and possible implications for earthquake prediction, *Nature*, **297**, 47–49.

Allègre, C. J., Shebalin, P., Le Mouël, J. L. & Narteau, C. 1998, Energetic balance in scaling organization of fracture tectonics, *Phys. Earth Planet. Int.*, **106**, 139–153.

Bak, P. & Tang, C., 1989, Earthquakes as a self-organized critical phenomenon, *J. Geophys. Res.*, **94**, 15635–15637.

Bâth, M., 1974, *Spectral analysis in geophysics*. Elsevier.

Ben-Zion, Y., 1996, Stress, slip and earthquakes in models of complex single-fault systems incorporating brittle and creep deformations, *J. Geophys. Res.*, **101**, 5677–5706.

Binney, J.J., Dowrick, N.J., Fisher, A.J. & Newman, M.E.J., 1992, *The theory of critical phenomena, an introduction to the renormalization group*, Oxford.

Blanter, E. M., Shnirman, M. G. & Le Mouël, J. L., 1997, Hierarchical model of seismicity: scaling and predictability, *Phys. Earth Planet. Int.*, **103**, 135–150.

Brune, J. N., 1968, Seismic moment, seismicity and rate along major fault zones, *J. Geophys. Res.*, **73**, 777–784.

Burridge, R. & Knopoff, L. 1967, Model and theoritical seismicity, *Bull. Seism. Soc. Am.*, **57**, 341–371.

Campillo, M. & Ionescu, I. R., 1997, Initiation of antiplane shear instability under slip dependent frictiong, *J. Geophys. Res.*, **102**, 20263–20271.

Chen, K., Bak, P. & Obukhov S. P., Self-organized criticality in a crack-propagation model of earthquakes, 1991, *Phys. Rev. A*, **43**, 625–630.

Cochard, A. & Madariaga, R., 1994, Dynamic faulting under rate-dependent frictions, *Pure Appl. Geophys.*, **142**, 419–445.

Correig, A. M., Urquizú, M. & Vila, J., 1997, Aftershock series of event february 18, 1996: An interpretation in terms of self-organized criticality, *J. Geophys. Res.*, **102**, 407–427.

Dieterich, J., 1979, Modelling of rock friction: 1.Experimental results and constitutive equations, *J. Geophys. Res.*, **84**, 2161–2168.

Dieterich, J., 1994, A constitutive law for rate of earthquake production and its application to earthquake clustering, *J. Geophys. Res.*, **99**, 2601–2618.

Dubois, J. & Gvishiani, A., 1998, *Dynamic systems and dynamic classification problems in geophysical applications*, Springer, Berlin.

Ellsworth, W. L. & Beroza, G. C., 1995, Seismic evidence for an earthquake nucleation phase, *Nature*, **268**, 851–854.

Fedotov, S. A., 1965, Regularities in the distribution of strong earthquakes in Kamchatka, the Kuriles, and Northern Japan, *Akad. Nauk USSR. Inst. Fiz. Zeml.*, **36**, 66–95.

Gross, S. & Rundle J., A systematic test of time-to-failure analysis, *Geophys. J. Int.*, **133**, 57–64.

Gutenberg, B. & Richter, C., 1944, Frequency of earthquakes in California, *Bull. Seismol. Soc. Am.*, **34**, 185–188.

Hainzl, S., Zöller, G. & Kurths, J. 1999, Similar power-laws for fore- and aftershock sequences in a spring-block model of earthquakes, *J. Geophys. Res.*, **104**, 7243–7254.

Harris, R. A., 1998, Introduction to special section: stress triggers, stress shadows, and implications for seismic hazard, *J. Geophys. Res.*, **103**, 24347–24358.

Kanamori, H. & Anderson, D. L. 1975, Theoritical basis of some empirical relations in seismology, *Bull. Seism. Soc. Am.*, **65**(5), 1073–1095.

King, G., 1983, The accomodation of large strain in the upper lithosphere of the Earth and other solids by self similar fault systems, *Pure Appl. Geophys.*, **121**, 761–815.

Knopoff, L., 1997, October, The physics of earthquakes. *Fourth Workshop on Non-linear Dyamics and Earthquake Prediction*, Trieste, Italy.

Kostrov, V. V., 1974, Seismic moment and energy of earthquakes, and seismic flow of rocks, *Phys. Solid Earth*, **1**, 23–44.

Kulldorf, G., 1961, *Contribution to the theory of estimation rank grouped and partially grouped samples*, Almquist and Wiksell, Stockholm-Göteborg-Uppsala.

Lee, W. H. K., 1997, *Algorithms for earthquake statistics and prediction.* IASPEI Software Library.

Main, I. G., Meredith, P. G., Sammonds, P. R. & Jones, C., 1990, Influence of fractal flaw distribution rock deformation in the brittle field, *Geol. Soc. London Special Publication*, **54**, 81–96.

Main, I. G., 1996, Statistical physics, seismogenics, and seismic hazard, *Rev. Geophys.*, **34**, 433–462.

Main, I. G., 1997, Long odds on prediction, *Nature*, **385**, 19–20.

Marrone, C., 1998, The effect of loading rate on static friction and the rate of fault healing during the earthquake cycle, *Nature*, **391**, 69–72.

Marrone, C. & Scholz, C. H., 1988, The depth of seismic faulting and the upper transition from stable to

unstable slip regimes, *Geophys. Res. Lett.*, **15**, 621–624.

Molchan, G., Kronrod, T. & Panza, G., 1997, Multi-scale seismicity model for seismic risk, *Bull. Seism. Soc. Am.*, **87**(5), 1220–1229.

Okada, Y., 1985, Surface deformation due to the shear and tensile faults in a half space, *Bull. Seism. Soc. Am.*, **75**, 1135–1154.

Okada, Y., 1992, Internal deformation due to shear and tensile faults in a half-space, *Bull. Seism. Soc. Am.*, *82*, 1018–1040.

Omori, F., 1894, On after-shocks of earthquakes, *J. Coll. Sci. Imp. Univ. Tokyo*, **7**, 111–200.

Otsuka, M., 1985, Physical interpretation of Omori's formula, *Sci. Rep. Shimabara Earthq. Volcano Obs.*, **13**, 11–20.

Papazachos, B., 1975, Foreshocks and earthquake prediction, *Tectonophysics*, **28**, 213–226.

Rice, J. R. & Ben-Zion, Y., 1996, Slip complexity in earthquake faults models, *Proc. Natl. Acad. Sci. USA*, **931**, 3811–3818.

Sammonds, P. R., Meredith, P. G. & Main, I. G., 1992, Role of pore fluids in the generation of seismic precursors to shear fracture, *Nature*, **359**, 228–230.

Scholz, C. H., 1998, Earthquakes and friction laws, *Nature*, **391**, 37–41.

Scholz, C. H., 1990, *The mechanism of earthquakes and faulting*, Cambridge University Press.

Shnirman, M. G. & Blanter, E. M., 1999, Mixed hierarchical model of seismicity: scaling and prediction, *Phys. Earth Planet. Int.*, **111**, 295–303.

Smith, W.D., 1981, The b-value as an earthquake precursor, *Nature*, **289**, 136–139.

Tapponnier, P. & Brace, W. F., 1976, Development of stress-induced microcracks in Westerly granite, *Mech. Min. Sci. Geomech. abstr.*, **131**, 103–112.

Tse, S. & Rice, J., 1986, Crustal earthquake instability in relation to the depth variation of friction slip properties, *J. Geophys. Res.*, **915**, 9452–9472.

Turcotte, D. L., 1999, Seismicity and self-organized criticality, *Phys. Earth Planet. Int.*, **111**, 275–293.

Utsu, T., Ogata, Y. & Matsu'ura, R., 1995, The centenary of the Omori formula for a decay law of aftershocks activity, *J. Phys. Earth*, **43**, 1–33.

Yamashita, T. & Ohnaka, M., 1991, Nucleation process of unstable rupture in the brittle regime: a theoritical approach based on experimentally inferred relations, *J. Geophys. Res.*, **96**, 8351–8367.

LIST OF FIGURES

1 Abstract representation of a fault zone: opposite tectonic motions on both sides of the fault zone generate an increase of the micro-cracks density. We study the different scales rupture phenomena through a hierarchical system. Here we draw the used hierachical system with $\mathcal{D} = 2$ and $\mathcal{R} = 2$.

2 Different possible states of a cell and possible transitions. Note that the $s \rightarrow b$ and the $m \rightarrow s$ transitions are forbidden.

3 The critical configurations of the S.O.F.T. rule ($\mathcal{D} = 2, \mathcal{R} = 2$). In brackets the number of critical configurations for a given number of broken or moving cells. The arrow indicates the "main direction".

4 Typical stress redistribution pattern generated by the motion of the central cell (subject itself to a stress change A_3) (for any level k). The shear stress increases along the main direction ($A_1 > A_0 > 0$) and decreases along the other direction ($A_2 < 0$).

5 Ideal propagation of the friction (from left to right) in a one dimensional hierachical system ($N = \mathcal{R}^K$). The t_i are the fracturation times of cells C_i and $t_i < t_j$ if $i < j$. Depending on the value of $(t_N - t_1)$ one obtains different kinds of seismic events (see text).

6 The reference sequence of the friction model in a linear time scale (a) and a logarithmic one (b). From top to bottom: the sequence of events, the total transition rate, the average shear stress, the standard deviaton of the local shear stress, and the density of moving cells at the elemenrtary level.

7 (a) cumulated number of aftershocks of the reference sequence versus a logarithmic time scale and the curve representative of the modified Omori law (eq. 30); (b) cumulative number of aftershocks of the reference sequence versus the theoretical number (straight line).

8 Magnitude-frequency law of the reference sequence : number of events (full line, $b = 1.85$), number of foreshocks (dotted line, $b = 1.43$), and number of aftershocks (dashed line, $b = 2.06$) versus the hierarchical level (or magnitude c.f. eq. 28).

9 Evolution of the b-value during the reference sequence. b-value is computed for consecutive time spans each containing 200 events.

10 More complex sequences: (a) a seismic quiescence a few seconds after the main shock (parameters values of the reference sequence except for $\theta^b = 1.5$); (b) a swarm of large earhquakes. From top to bottom in logarithmic time scale: the events sequence, the total transition rate and the average shear stress (parameters values of the reference sequence except for $\lambda^b = 20$ bars). Note that the modified Omori law is still respected in these two cases.

11 (a) the cumulative number of aftershocks versus time in a logarithmic scale and the curve representative of the modified Omori law (eq. 30). (b) the cumulative number of aftershocks obtained in the numerical experiment versus the theoretical one (straight line). Parameters values of the reference sequence except for $\mathcal{D} = 3$.

12 Experiment with different numbers of levels: left side graphs show the events sequences versus time; right side graphs represent the cumulative number of aftershocks versus time in a logarithmic scale and the representative curve of the Otsuka law (eq. 31) for estimated p and T parameters (parameters values of the reference sequence except for $\lambda^b = 5$ bars).

13 Examples of creep sequences. From top to bottom the sequence of events, the total transition rate, the average shear stress, the standard deviaton of the local shear stress and the density of moving cells at the elementary level. (a) is for the "weak" state with $\sigma_a < \sigma_b$ (parameters values of the reference sequence except for $E = 10^{-4}$ bars s^{-1}); (b) for the "strong" state with $\sigma_a > \sigma_b$ (parameters values of the reference sequence except for $E = 10^{-2}$ bars s^{-1}).

14 Examples of seismic cycles obtained with the parameters values of the reference sequence and homogeneisation by diffusion (see text). From top to bottom: the sequence of events, the total transition rate, the average shear stress, the standard deviaton of the local shear stress and the density of moving cells.

15 Intermediate sequences of earthquakes: (a1), (b1), (b2), (b3), (c1), (d1), (e1). Average shear stress versus time: (d2), (c2), (e2). Number of solid cells versus time: (a3).

16 (a1) is a main shock-aftershocks sequence. (a2) and (a3) show respectively the corresponding evolution versus time of the average stress and of the number of solid cells. (a4) shows the cumulated number of aftershocks in a logarithmic time scale and a representative curve of the modified Omori law (eq. 30). (a5) shows the cumulative number of aftershocks versus the theoretical one (straight line).

17 The cumulative number of aftershocks versus time in a logarithmic scale calculated from a critical configuration of broken cells at the elementary level (the highest level cell is broken) and without stress redistribution ($\lambda = 0$), without healing ($\beta = 0$), without external loading ($E = 0$): (a) all the solid cells have the same local stress $\sigma_h > \sigma_s$; (b) the average stress of all the solid cells is σ_h, but, for each individual solid cell, the stress is randomly chosen in $[\sigma_s; \sigma_s + 2\sigma_h]$. The best fitting curve is plotted and its formula is written ((a) gives an exponential frequency decay; (b) a $(1/(t+c)^p)$ frequency decay).

18 (a1), b(1): exemple of complete foreshocks sequences with a linear time scale (parameters values set of Tab. 1 **A** and **B** with different initial conditions; see text). (a2), (b2): the sequences of the selected foreshocks in a logarithmic time scale. (a3), (b3): the cumulated number of foreshocks in a logarithmic time scale and a theoretical estimate from the modified Omori law (eq. 30); (a4), (b4): the cumulative number of foreshocks versus the theoretical one (straight line).

19 The magnitude-frequency relationship for all events (solid line), for main shocks only (dashed line), for aftershocks of main shocks of level $\mathcal{K}$ (dotted-dashed line), for aftershocks of main shocks of level $\mathcal{K} - 1$ and $\mathcal{K} - 2$ (dotted lines). Calculated b-value are indicated.

20 Versus δ_s: (a) the average value and standard deviation of the parameter p of eq. 30 compiled from a large number of aftershocks sequence ($\sim 10^3$; we run the model for a very long time to get this large number) , (b) the average value of the parameter c of eq. 30, (c) the average number of aftershocks and the standard deviation of this number , (d) the average b-value.

21 Evolution of b-value (a) and of f value (b)(see text), versus the average density of fractures at the lowest level. Open circles are from numerical experiments with different values of E and β (see text), while the solid line is calculated from the integral approach (if f_l and d_l are respectively the events frequency and the cracks density at level l, the events frequency at the higher level is $f_{l+1} = f_l(1 - d_{l+1})(1 - (1 - d_l^2)^2)$).

22 Evolution versus E/β of (a) f, the ratio between the total (all over the whole sequence) stress dissipated by the "fracturation" process and the total stress dissipated by the "friction" process, (b) the b-value and (c) the density of fractures at the lowest level.

23 (a) evolution of parameter Q versus E/β. (b) evolution of b-value versus Q.

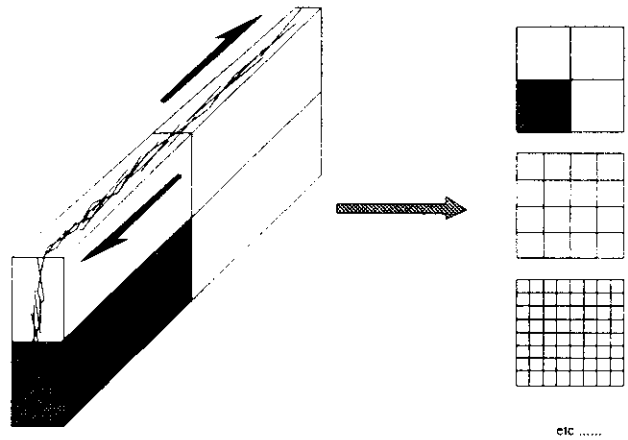

Figure 1. Abstract representation of a fault zone: opposite tectonic motions on both sides of the fault zone generate an increase of the micro-cracks density. We study the different scales rupture phenomena through a hierarchical system. Here we draw the used hierachical system with $\mathcal{D} = 2$ and $\mathcal{R} = 2$.

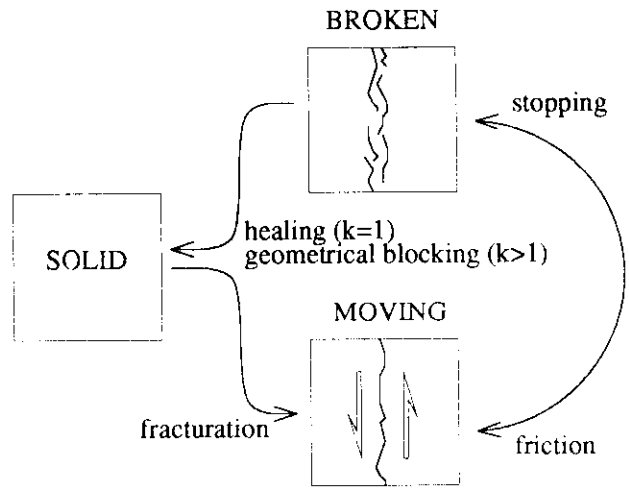

Figure 2. Different possible states of a cell and possible transitions. Note that the $s \rightarrow b$ and the $m \rightarrow s$ transitions are forbidden.

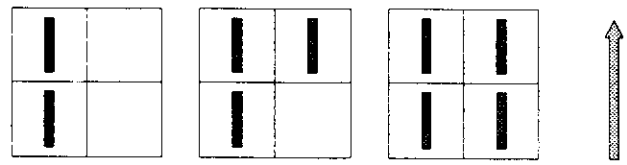

Figure 3. The critical configurations of the S.O.F.T. rule ($\mathcal{D} = 2$, $\mathcal{R} = 2$). In brackets the number of critical configurations for a given number of broken or moving cells. The arrow indicates the "main direction".

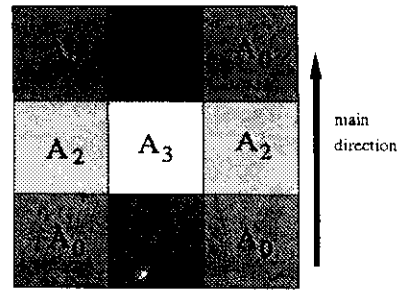

Figure 4. Typical stress redistribution pattern generated by the motion of the central cell (subject itself to a stress change A_3) (for any level k). The shear stress increases along the main direction ($A_1 > A_0 > 0$) and decreases along the other direction ($A_2 < 0$).

Figure 5. Ideal propagation of the friction (from left to right) in a one dimensional hierachical system ($N = \mathcal{R}^K$). The t_i are the fracturation times of cells C_i and $t_i < t_j$ if $i < j$. Depending on the value of $(t_N - t_1)$ one obtains different kinds of seismic events (see text).

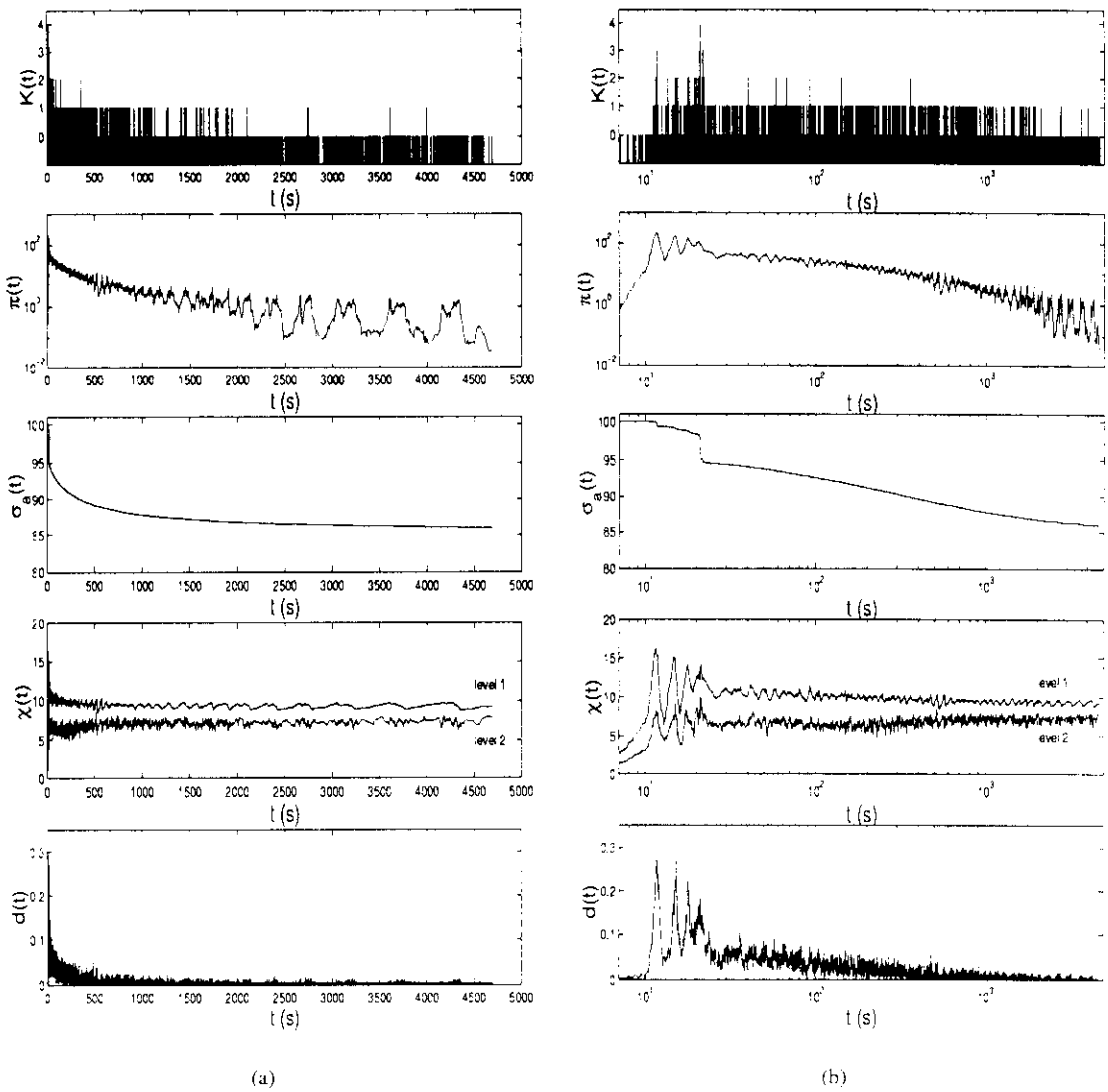

Figure 6. The reference sequence of the friction model in a linear time scale (a) and a logarithmic one (b). From top to bottom: the sequence of events, the total transition rate, the average shear stress, the standard deviaton of the local shear stress, and the density of moving cells at the elemenrtary level.

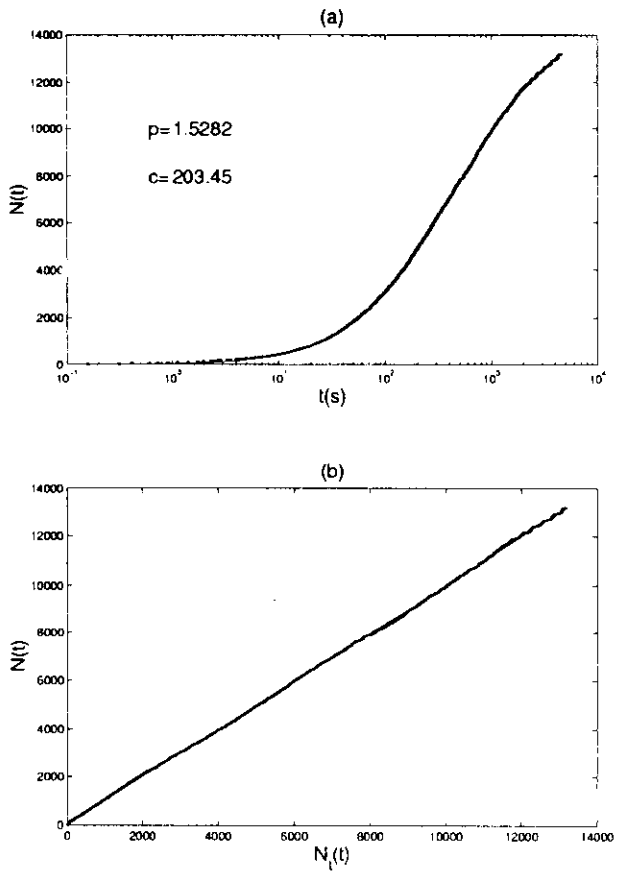

Figure 7. (a) cumulated number of aftershocks of the reference sequence versus a logarithmic time scale and the curve representative of the modified Omori law (eq. 30); (b) cumulative number of aftershocks of the reference sequence versus the theoretical number (straight line).

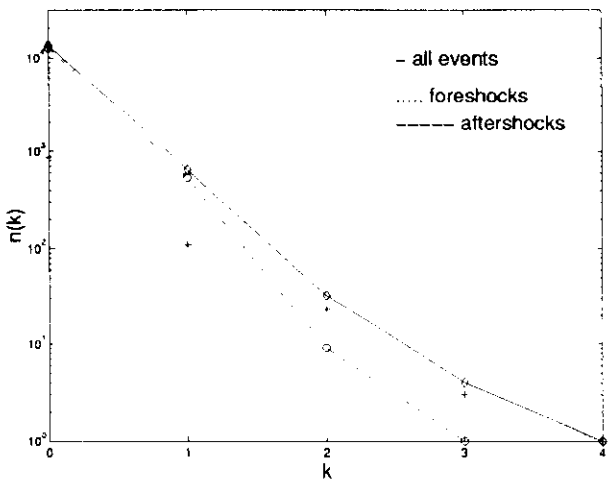

Figure 8. Magnitude-frequency law of the reference sequence : number of events (full line, $b = 1.85$), number of foreshocks (dotted line, $b = 1.43$), and number of aftershocks (dashed line, $b = 2.06$) versus the hierarchical level (or magnitude c.f. eq. 28).

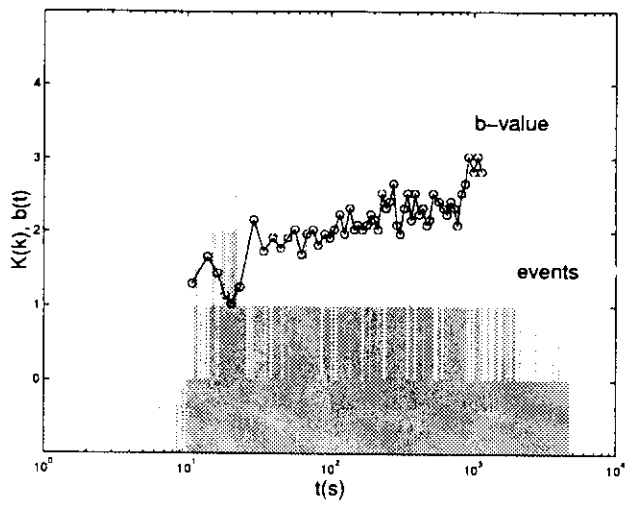

Figure 9. Evolution of the b-value during the reference sequence. b-value is computed for consecutive time spans each containing 200 events.

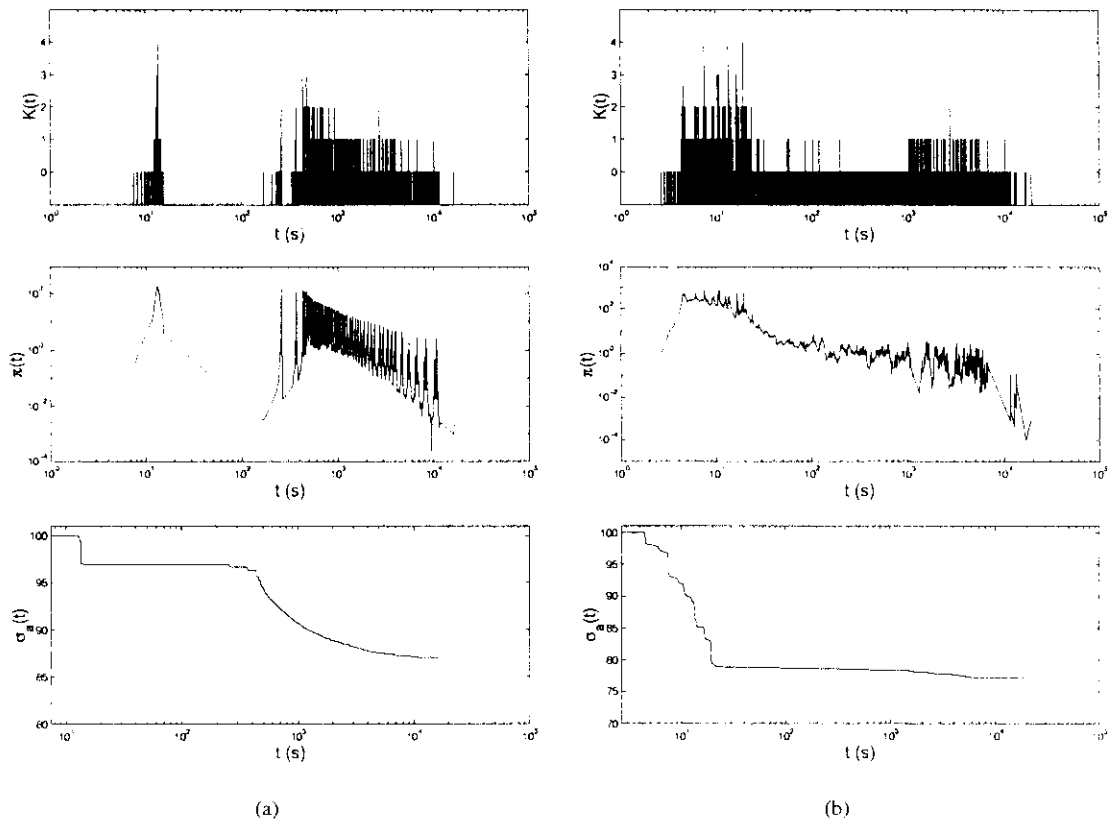

Figure 10. More complex sequences: (a) a seismic quiescence a few seconds after the main shock (parameters values of the reference sequence except for $\theta^b = 1.5$); (b) a swarm of large earthquakes. From top to bottom in logarithmic time scale: the events sequence, the total transition rate and the average shear stress (parameters values of the reference sequence except for $\lambda^b = 20$ bars). Note that the modified Omori law is still respected in these two cases.

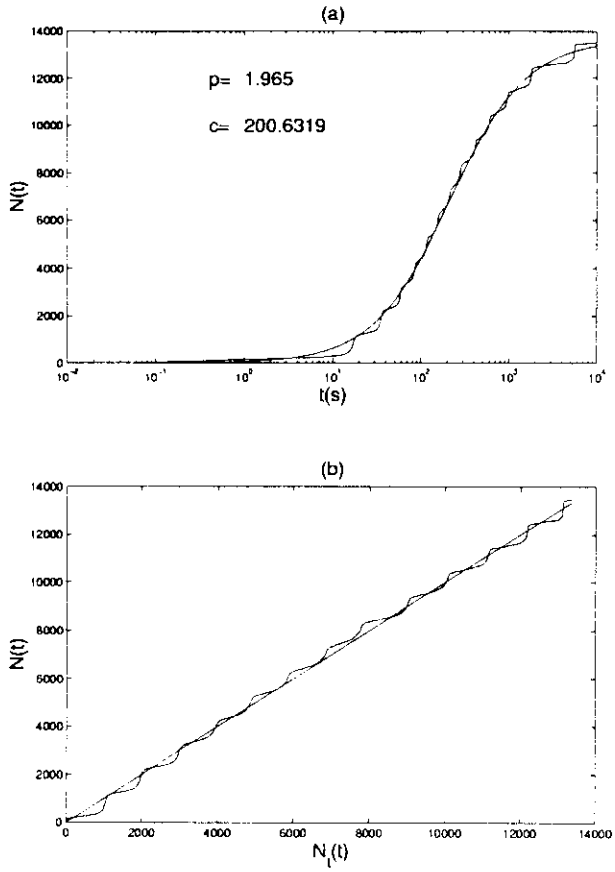

Figure 11. (a) the cumulative number of aftershocks versus time in a logarithmic scale and the curve representative of the modified Omori law (eq. 30). (b) the cumulative number of aftershocks obtained in the numerical experiment versus the theoretical one (straight line). Parameters values of the reference sequence except for $\mathcal{D} = 3$.

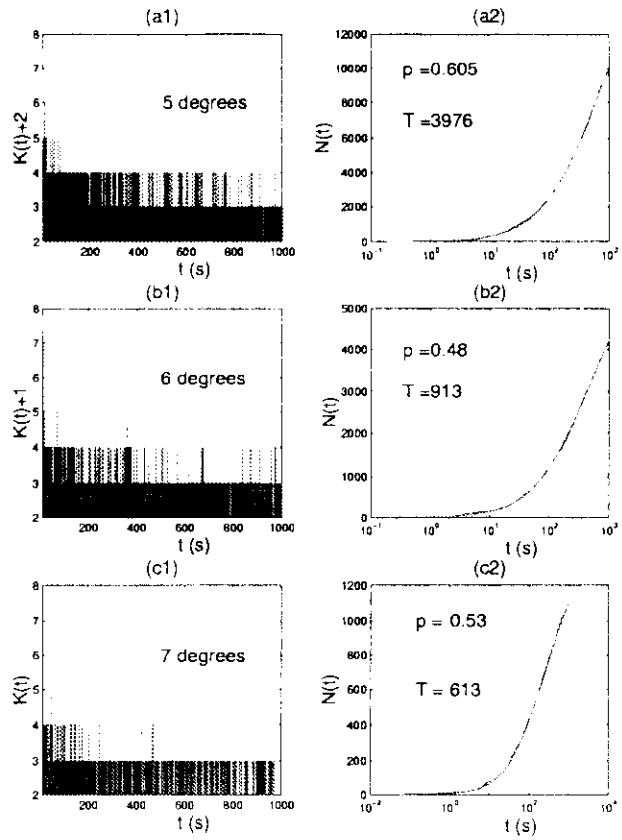

Figure 12. Experiment with different numbers of levels: left side graphs show the events sequences versus time; right side graphs represent the cumulative number of aftershocks versus time in a logarithmic scale and the representative curve of the Otsuka law (eq. 31) for estimated p and T parameters (parameters values of the reference sequence except for $\lambda^b = 5$ bars).

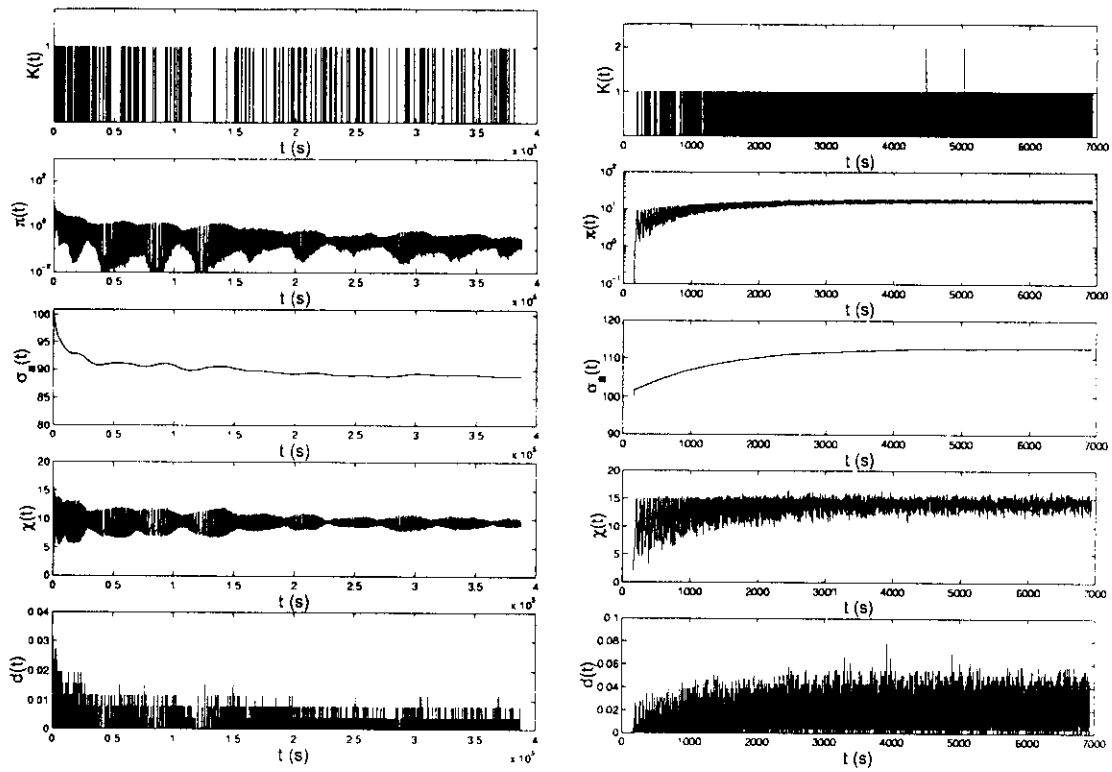

Figure 13. Examples of creep sequences. From top to bottom the sequence of events, the total transition rate, the average shear stress, the standard deviaton of the local shear stress and the density of moving cells at the elementary level. (a) is for the "weak" state with $\sigma_a < \sigma_b$ (parameters values of the reference sequence except for $E = 10^{-4}$ bars s^{-1}); (b) for the "strong" state with $\sigma_a > \sigma_b$ (parameters values of the reference sequence except for $E = 10^{-2}$ bars s^{-1}).

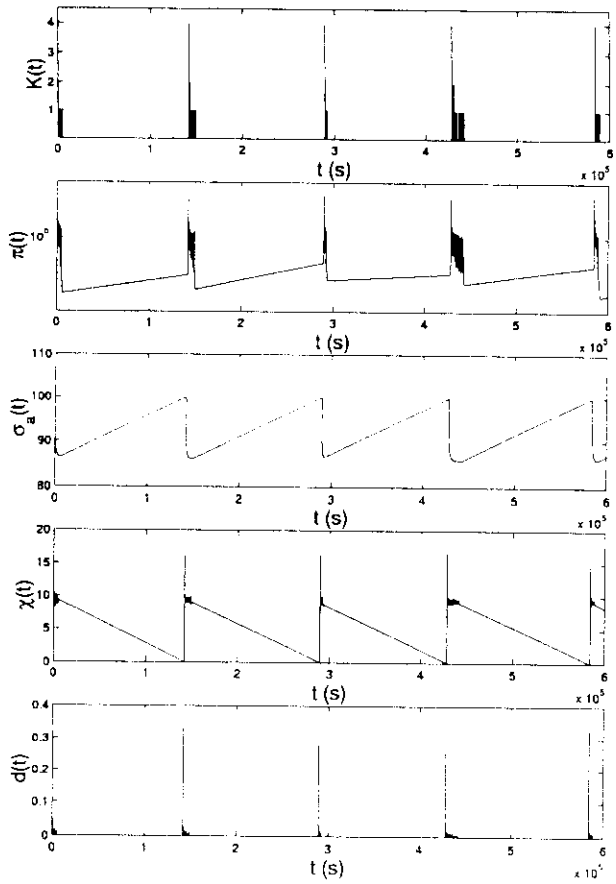

Figure 14. Examples of seismic cycles obtained with the parameters values of the reference sequence and homogeneisation by diffusion (see text). From top to bottom: the sequence of events, the total transition rate, the average shear stress, the standard deviaton of the local shear stress and the density of moving cells.

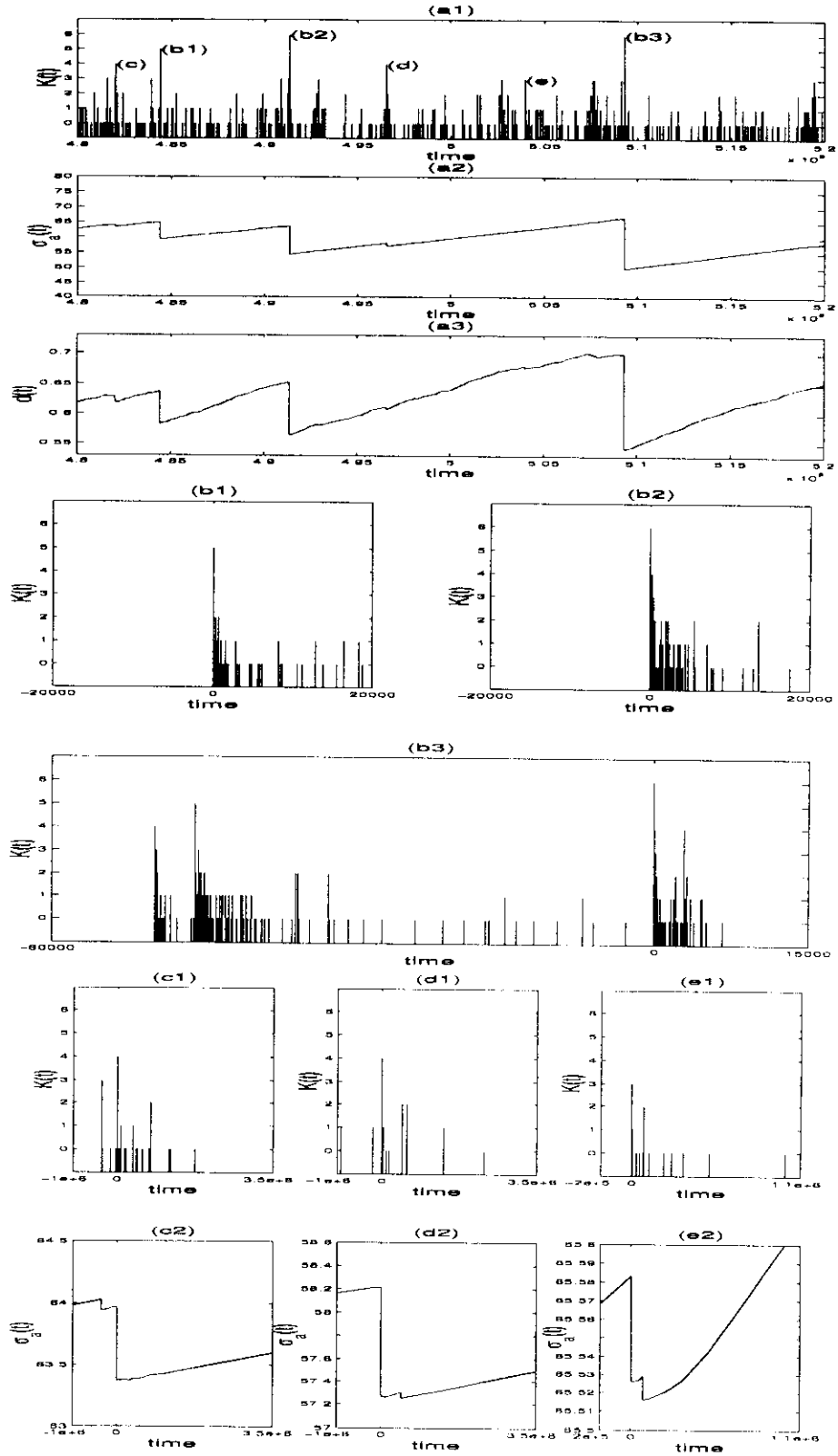

Figure 15. Intermediate sequences of earthquakes: (a1), (b1), (b2), (b3), (c1), (d1), (e1). Average shear stress versus time: (d2), (c2), (e2). Number of solid cells versus time: (a3).

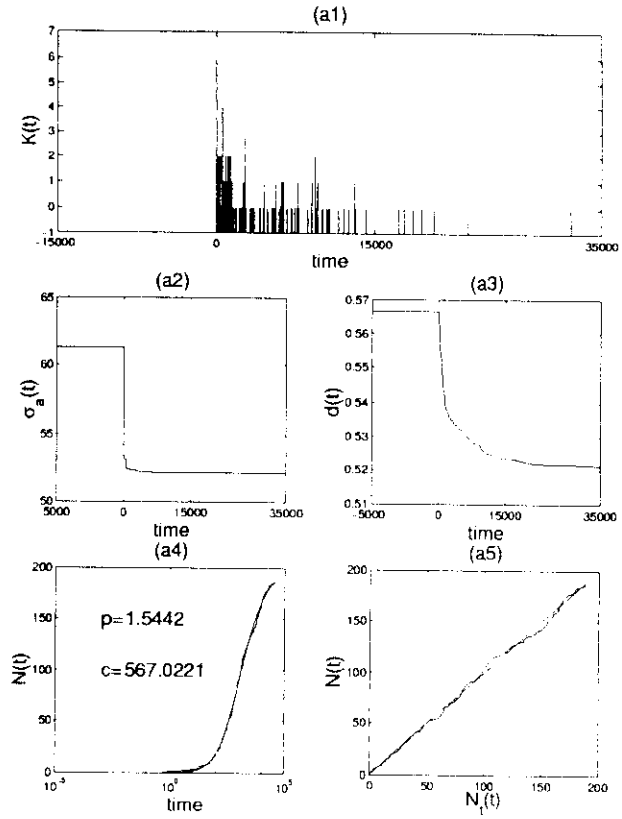

Figure 16. (a1) is a main shock-aftershocks sequence. (a2) and (a3) show respectively the corresponding evolution versus time of the average stress and of the number of solid cells. (a4) shows the cumulated number of aftershocks in a logarithmic time scale and a representative curve of the modified Omori law (eq. 30). (a5) shows the cumulative number of aftershocks versus the theoretical one (straight line).

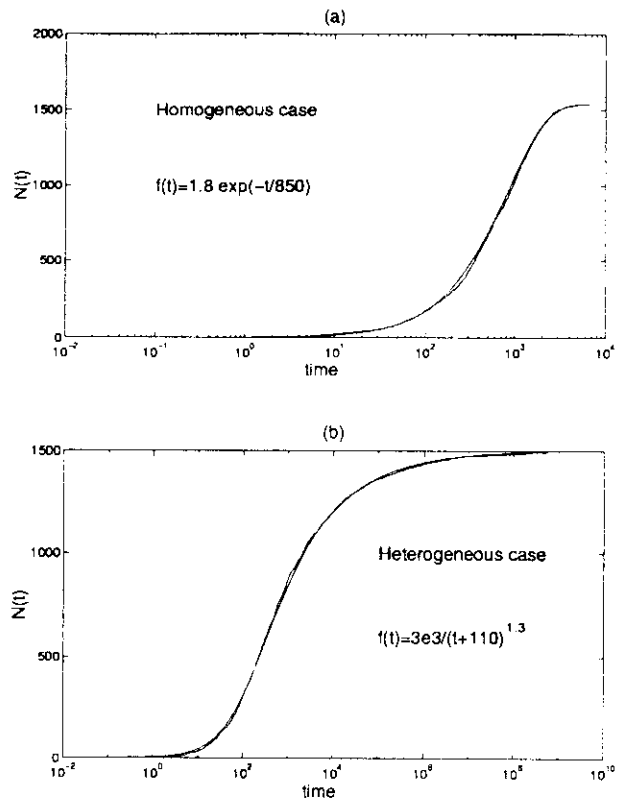

Figure 17. The cumulative number of aftershocks versus time in a logarithmic scale calculated from a critical configuration of broken cells at the elementary level (the highest level cell is broken) and without stress redistribution ($\lambda = 0$), without healing ($\beta = 0$), without external loading ($E = 0$): (a) all the solid cells have the same local stress $\sigma_h > \sigma_s$; (b) the average stress of all the solid cells is σ_h, but, for each individual solid cell, the stress is randomly chosen in $[\sigma_s; \sigma_s + 2\sigma_h]$. The best fitting curve is plotted and its formula is written ((a) gives an exponential frequency decay; (b) a $(1/(t+c)^p)$ frequency decay).

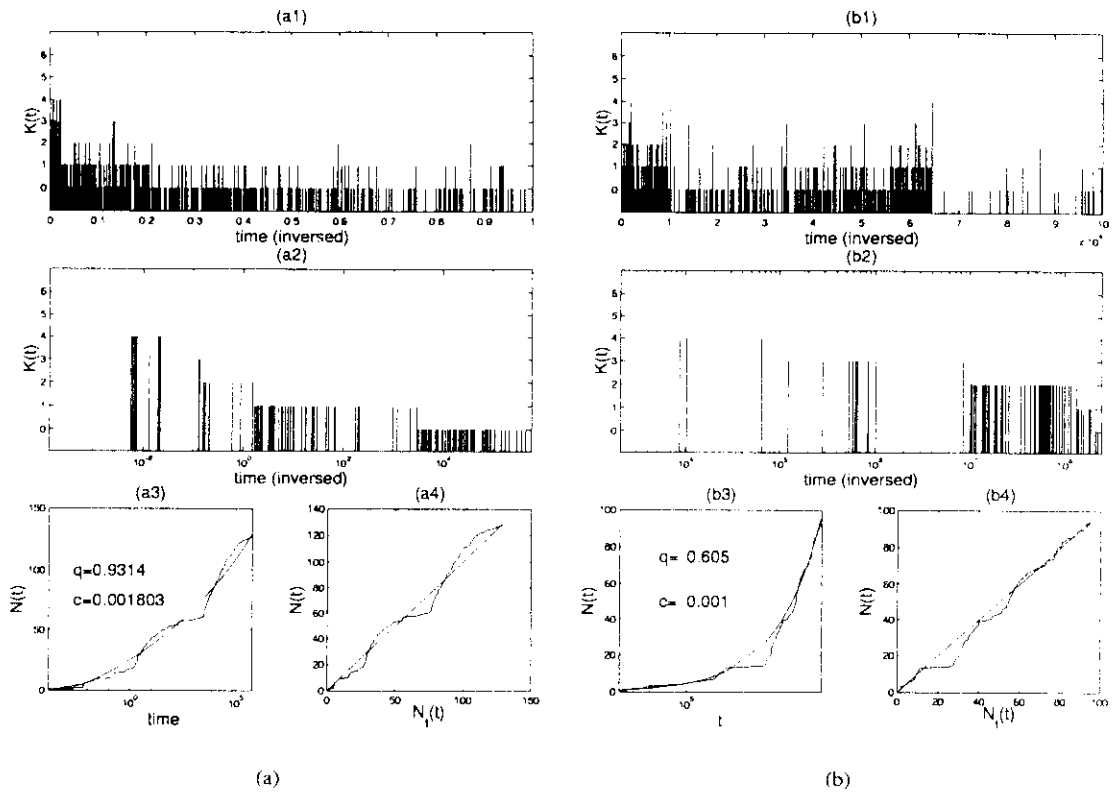

Figure 18. (a1), b(1): exemple of complete foreshocks sequences with a linear time scale (parameters values set of Tab. 1 **A** and **B** with different initial conditions; see text). (a2), (b2): the sequences of the selected foreshocks in a logarithmic time scale. (a3), (b3): the cumulated number of foreshocks in a logarithmic time scale and a theoretical estimate from the modified Omori law (eq. 30); (a4), (b4): the cumulative number of foreshocks versus the theoretical one (straight line).

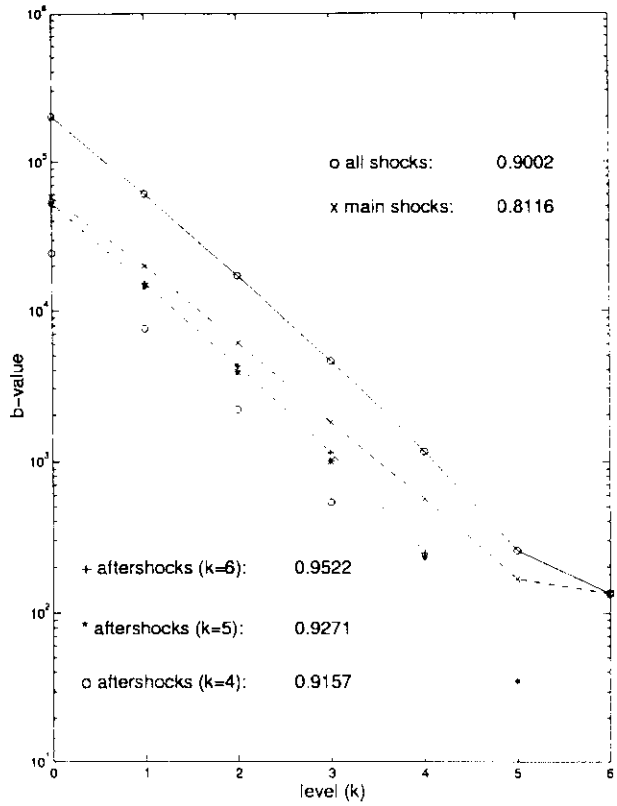

Figure 19. The magnitude-frequency relationship for all events (solid line), for main shocks only (dashed line), for aftershocks of main shocks of level K (dotted-dashed line), for aftershocks of main shocks of level $K-1$ and $K-2$ (dotted lines). Calculated b-value are indicated.

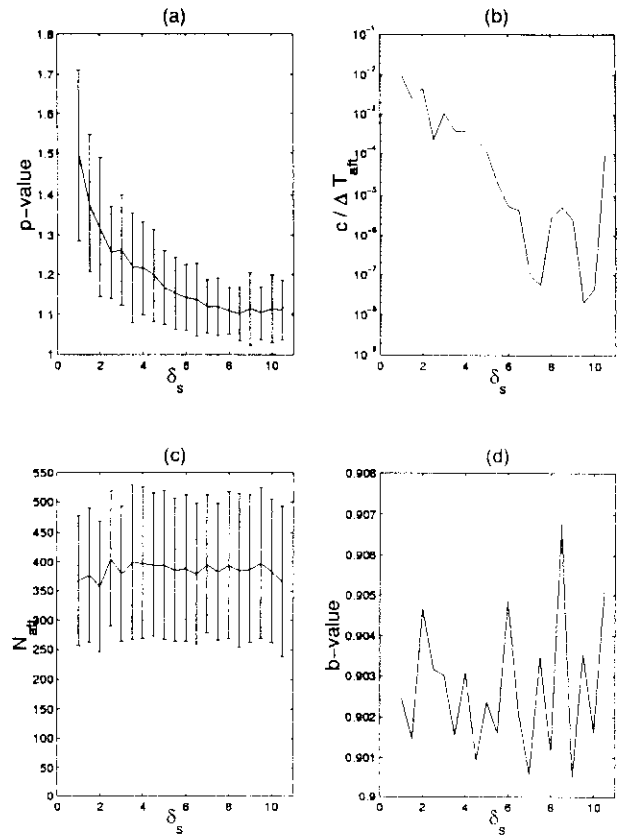

Figure 20. Versus δ_s: (a) the average value and standard deviation of the parameter p of eq. 30 compiled from a large number of aftershocks sequence ($\sim 10^3$; we run the model for a very long time to get this large number) , (b) the average value of the parameter c of eq. 30, (c) the average number of aftershocks and the standard deviation of this number , (d) the average b-value.

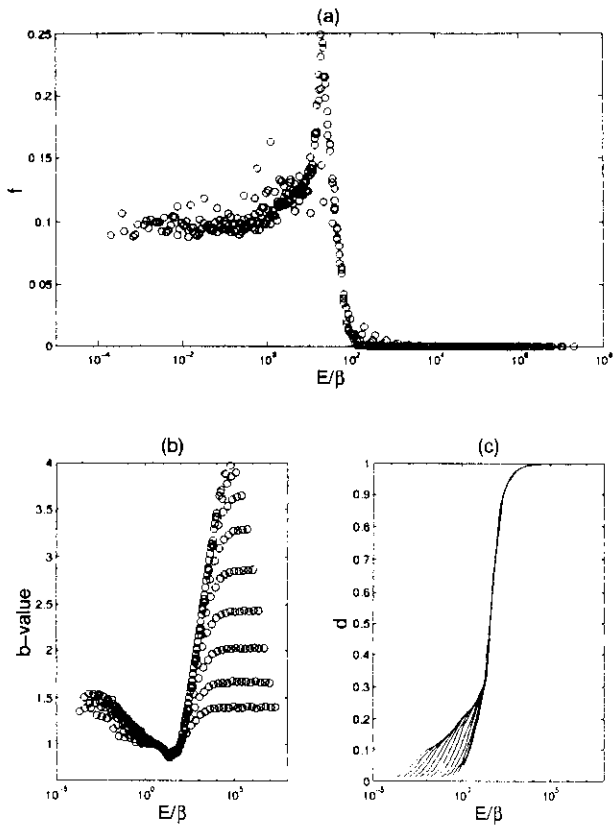

Figure 21. Evolution of b-value (a) and of f value (b)(see text), versus the average density of fractures at the lowest level. Open circles are from numerical experiments with different values of E and 3 (see text), while the solid line is calculated from the integral approach (if f_l and d_l are respectively the events frequency and the cracks density at level l, the events frequency at the higher level is $f_{l+1} = f_l(1 - d_{l+1})(1 - (1 - d_l^2)^2)$).

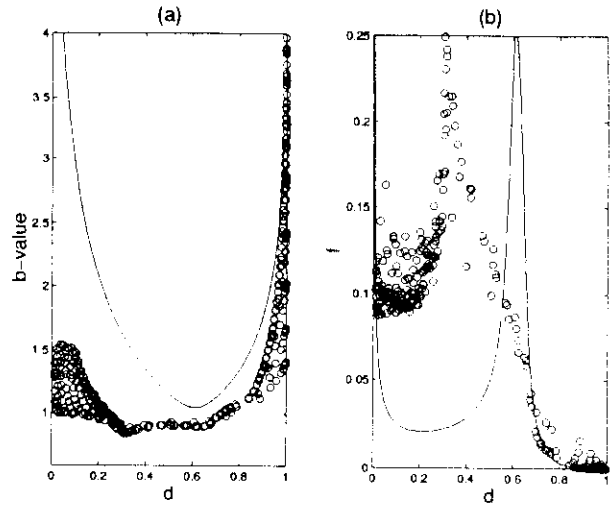

Figure 22. Evolution versus E/β of (a) f, the ratio between the total (all over the whole sequence) stress dissipated by the "fracturation" process and the total stress dissipated by the "friction" process, (b) the b-value and (c) the density of fractures at the lowest level.

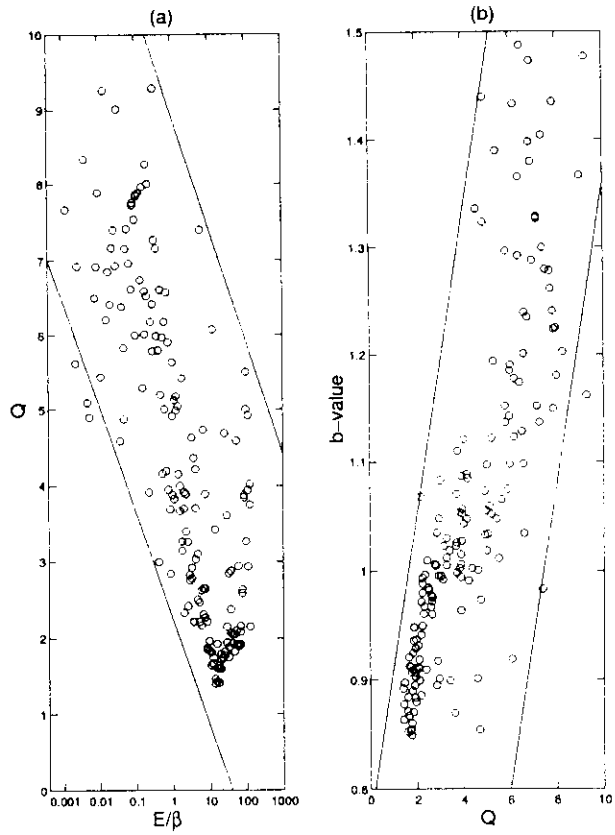

Figure 23. (a) evolution of parameter Q versus E/β. (b) evolution of b-value versus Q.

LIST OF TABLES

$\mathcal{R}$	2
$\mathcal{D}$	2
v_r	3000 ms^{-1}
σ_b	100 bars
σ_s	110 bars
$\Delta\sigma_{loc}$	30 bars
μ_2	$2\,\mathcal{R}^{\mathcal{D}\mathcal{K}}$ bars
E	10^{-9} bars s^{-1}
k_s	10^{-4} s^{-1}
δ_s	3
δ_b	1.5

table **A**

"fracturation" model	
$\mathcal{K}$	6
β	3.10^{-11} s^{-1}
k_b	$\rightarrow \infty$
θ^s	1.5
$A^s_{i=\{0,\ldots,3\}}$	1,2,-7,0
λ^s	5.8 10^{-2} bars
Initial Condition	completly solid
event	$s \rightarrow b$

table **B**

"friction" model	
$\mathcal{K}$	4
β	0
k_b	2.5 10^{-2} s^{-1}
θ^b	0.5
$A^b_{i=\{0,\ldots,3\}}$	1,2,-4,-8
λ^b	2 bars
Initial Condition	completly broken
event	m

table **C**

Table 1. Table **A**: Parameters which are kept constant in both model ($\Delta\sigma_{loc} = \Delta\sigma^s_{loc} = \Delta\sigma^b_{loc}$); table **B**: parameters of the "fracturation"model; table **C**: parameters of the "friction" model.